

**Behavior of a Container Drifted
by Run-up Tsunami
and Estimation Method of Its Collision Force**

Gyeong-Seon Yeom

Supervised by
Prof. Norimi Mizutani

Coastal & Ocean Engineering Laboratory
Department of Civil Engineering
Nagoya University
JAPAN

Acknowledgments

The author would like to thank his supervisor Prof. Norimi Mizutani, Nagoya University, for his detailed guidance and kind encouragement during doctoral course.

Special appreciation goes to this dissertation committee, which consisted of Prof. Norimi Mizutani, Nagoya University (Chari); Prof. Tetsuro Tsujimoto, Nagoya University; Koji Fujima, National Defense Academy; and Assoc. Prof. Koji Kawasaki, for their careful review and detailed comments.

The author believes that this dissertation could not be done without the help of former and present members of the Coastal & Ocean Engineering Laboratory, Nagoya University, for helpful discussions, suggestions, and constant support, and especially Assoc. Prof. Kwang-Ho Lee and Mr. Chang-Hoon Kim for valuable professional discussions and advisors.

The author also wishes to express his gratitude to Prof. Ki-Sung Bae, Gyeongsang National University, Korea; and Assoc. Prof. Dong-Soo Hur, Gyeongsang National University, Korea, for their constant encouragement.

This dissertation has been supported by the financial aid of the Japanese Government (Monbu-Kagaku-sho; Ministry of Education, Culture, Sports, Science and Technology) Scholarship Program. The author thanks for the financial support.

Last but not least, the author expresses his deepest gratitude to his wife Ms. Seo-Hui Lee and his family for devotion and encouragement in all aspects of his life.

Table of Contents

CHAPTER1	INTRODUCTION	1
1.1	Study Background	1
1.2	Literature Review	6
1.3	Study Objectives.....	8
1.4	Contents.....	10
CHAPTER2.	CHARACTERISTICS OF RUN-UP TSUNAMI AND BEHAVIOR OF DRIFTED CONTAINER	12
2.1	General	12
2.2	Experimental Setups.....	13
2.3	Experimental Results.....	18
2.3.1	Run-up wave level and fluid velocity	18
2.3.2	Behavior of drifted container.....	20
2.3.2.1	Continuous sea wall as a back-yard structure	22
2.3.2.2	Rectangular structures as a back-yard structure.....	24
2.3.3	Collision and wave forces.....	26
2.3.4	Importance of added mass	27
2.4	Remarks.....	28
CHAPTER3	REVIEW OF ESTIMATION FORMULA FOR COLLISION FORCE OF DRIFTED CONTAINER	30
3.1	General	30
3.2	Review of Estimation Formula.....	31
3.3	Improvement of Estimation Formula.....	33
3.4	Remarks.....	35
CHAPTER4	NUMERICAL MODEL	37
4.1	General	37
4.2	Drifting Model.....	38
4.2.1	Governing equations.....	39
4.2.2	Numerical schemes.....	41

4.3 Collision Model	44
4.3.1 Governing equations	44
4.3.2 Numerical scheme	47
4.3.2.1 Operating method	47
4.3.2.2 Mesh smoothing algorithm	48
4.3.2.3 Advection algorithm	49
4.3.2.4 Contact condition	50
4.4 Remarks	51
CHAPTER5 VALIDITY OF ESTIMATION FORMULA WITH NUMERICAL SIMULATION	52
5.1 General	52
5.2 Verification of Numerical Models	53
5.2.1 Drifting model	53
5.2.2 Collision model	58
5.2.3 Drifting collision coupled model	60
5.2.3.1 Determination of wave range behind container	60
5.2.3.2 Validity of coupled model	62
5.3 Determination of Incident Waves	69
5.4 Collision Forces as Changing Position	75
5.5 Drifting Velocity and Wave Level by Drifting Simulation	76
5.6 Comparison of Collision Forces by Collision Model and Estimation Formula	77
5.7 Remarks	79
CHAPTER6 APPLICABILITY OF ESTIMATION FORMULA TO PROTOTYPE CONDITIONS	81
6.1 General	81
6.2 Verification of Collision Model in Large Scale	81
6.3 Applicability of Estimation Formula to Actual Field	87
6.3.1 Revision of the modified estimation formula	87
6.3.2 Definition of collision force in actual phenomenon	88
6.3.3 Comparison of collision forces by collision model and revised estimation formula	91
6.4 Simplification of Estimation Formula	108
6.5 Remarks	114
CHAPTER7 CONCLUSION	116
Reference	121

CHAPTER 1

INTRODUCTION

1.1 Study Background

From old times, tsunamis have caused tremendous damages to human race. In 2004, Indonesia and other countries surrounding Indian Ocean were damaged by Sumatra tsunami. Tsunami is generally caused by the earthquakes generated by the fault movement along the ocean trenches. Countries bordering oceans with such trenches like Japan have high possibility to be attacked by the ocean earthquake tsunami. Representative past damages are introduced through cases of Japan as follows.

In 1896, around Sanriku coast was damaged i.e. more than 20,000 deaths and the presumed financial damage equivalent to 10% of Japanese national budget at that time by tsunami due to Meiji-Sanriku earthquake (The Central Disaster Prevention Committee of Cabinet Office, Government of Japan, 2005). This event triggered that the people lived away from the coastal line. On Showa-Sanriku tsunami in 1933, the life loss reduced by using previous experience, however tragedy 3,064 deaths was repeated (Photo 1.1). It was pointed out that a rias coast of this area is main reason for increasing tsunami damage. The difference in water depth and width between mouth and head of bay causes large wave height according to wave propagation. From this lesson, Iwate prefecture constructed the breakwater in length of 1,960m at Kamaishi bay using modern civil engineering technique to make up for the weak points in the topography under unfavorable condition which is the most deep water depth in the world, 63m, and that has protected the life and property of inhabitants until now.

These tsunami disasters have been occurred at not only Sanriku area but also other places in Japan. In 1993, a tsunami occurred by Hokkaido-Nanseioki earthquake had attacked Okushiri island, Hokkaido. Especially, on Aonae area surrounded with sea in three faces, destruction of structures as well as large scale fire due to earthquake and tsunami were generated, consequently the village was destroyed totally (Photo 1.2). The characteristic of this tsunami was an early arrival that is 3-5min from occurrence of



(a) Before tsunami attack



(b) After tsunami attack

Photo 1.1 Damage on Tarou-cho, Shimohei-gun, Iwate prefecture by Showa-Sanriku earthquake tsunami in 1933 (National Diet Material Compilation Committee of Japan, 1998)

earthquake to arrival of first wave. Due to that reason, people were hard to refuge to an elevated place. At present, a steel framed reinforced concrete tsunami refuge terrace in height of 6m was constructed to rapid refuge of the persons concerned with fishery in Aonae fishery port (Photo 1.3).



Photo 1.2 Damage on Okushiri island by Hokkaido Nanseioki earthquake tsunami in 1993
(National Diet Material Compilation Committee of Japan, 1998)



Photo 1.3 Tsunami refuge terrace at Aonae fishery port

Source: <http://www.town.okushiri.lg.jp/>

Tokai area is the most concerned area to capable of trench earthquake in Japan. Historically, the earthquakes have reoccurred in roughly the same place and with a similar magnitude along Tokai area to Shikoku in a cycle of about one every 100 to 150 years as shown in Fig. 1.1. About 90 years after Ansei-Nankai and Ansei-Tokai earthquakes, Tonankai earthquake and Nankai earthquake occurred, and earthquake

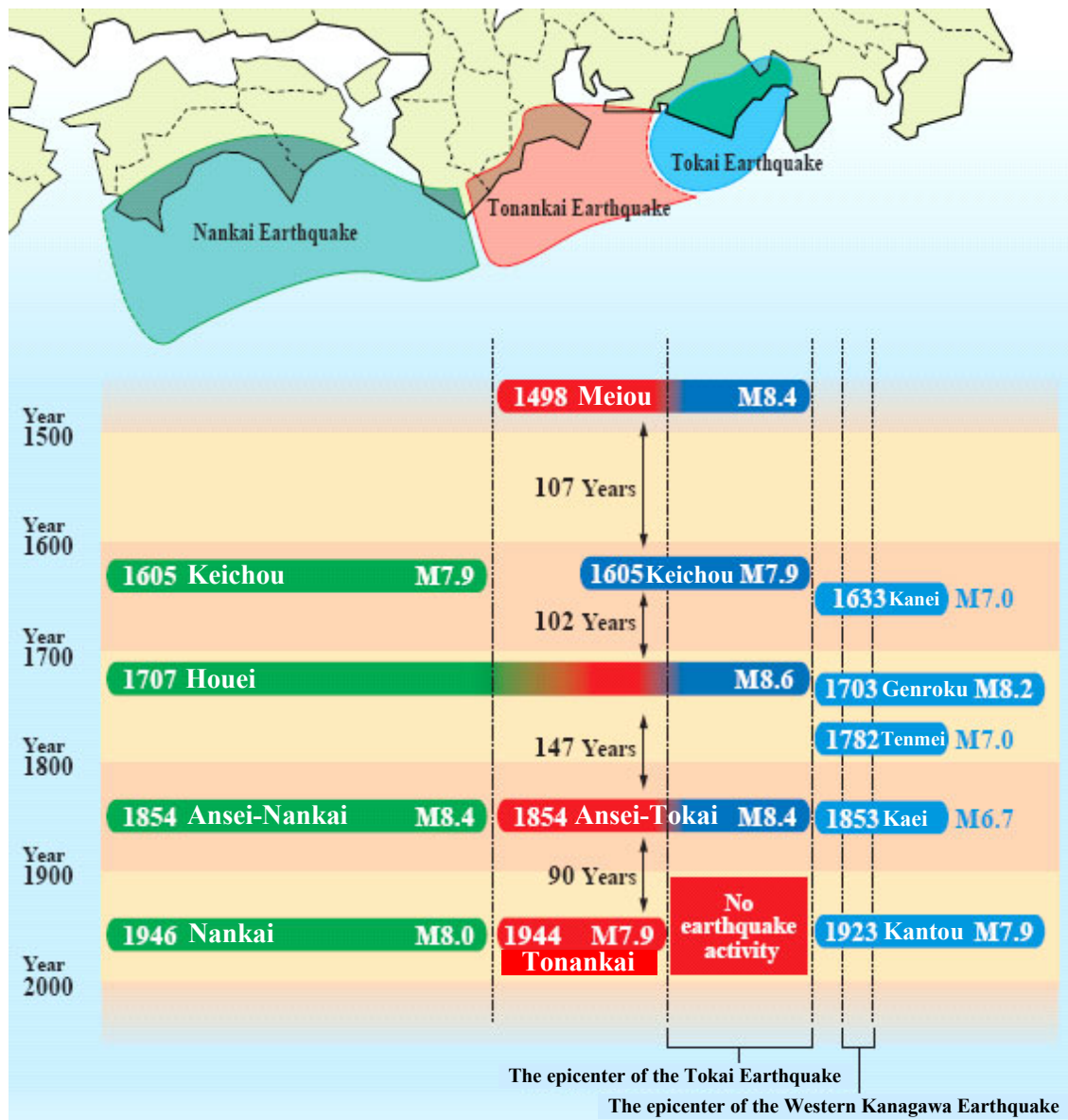


Fig. 1.1 Past earthquakes occurring off the Pacific coast and their estimated epicenters

Source: <http://www.pref.shizuoka.jp/bousai/>

energy was released by these earthquakes. In Tokai area, however, the earthquake has not been occurred yet. It is believed that earthquake energy is building up in this area. Because of this blank of observed earthquake activity, a massive earthquake is expected to occur in Tokai area in the near future.

Japan, an island country, has numerous trading and fishery ports all over the country, as well as cargo amount is also increasing according to economic growth. At present, 99.7% in weight and 69.7% in worth of the total volume of trade are dealt via the port, and the port became one of the important infrastructures in our life. The main current of the freight in the world is container which is portable, besides increasing the volume of



Photo 1.4 Tobishima container terminal in Nagoya port

Source: <http://www.nptc.or.jp/>

dealings is also expected in Japan. Other countries are increasing the volume of dealings of container using restructuring of container terminal, and Japan is also restructuring the major five ports. As the beginning, Nagoya port is restructuring in soft and hard ways (Photo 1.4).

When a tsunami attacks ports where cargoes are transported and numerous people are working, not only direct damages such as human loss, inundation, and destruction of structures by run-up waves but also indirect damages caused by drifted bodies such as containers, lumbers, vessels, vehicles, and destroyed debris are predicted. Furthermore, it should be concerned about the indirect damages which bodies drifted by run-up waves collide with other back-yard structures and fall into sea route or berth. In this case, the port can not be used in transporting emergency materials to repair and revival. As an instance, on Hanshin-Awaji earthquake in 1995, almost port facilities in Kobe were damaged consequently the whole Japan economy had been affected. Ports are very important part in national economic activities as mentioned above, and therefore we should prevent and reduce the damages by natural disasters such as tsunamis. Thus, the prediction of characteristics such as wave force, and behavior of drifted bodies and collision force by drifted bodies in tsunami disasters is essential in establishing countermeasures.

1.2 Literature Review

Because of frequent occurrence of tsunami in Japan, world top class studies on the tsunami have been performed. As representative results, there is giving tsunami warning and advisory. It is well known that the mass media announce an estimated tsunami height and arrival time of tsunami to the people immediately after occurrence of earthquake. Furthermore, the central disaster prevention committee of cabinet office, government of Japan estimated the expected epicenter area, seismic intensity and tsunami heights at each place of the Tokai earthquake which is predicted to occur, and those are being used as the data for establishing various countermeasures. While these are famous examples of the tsunami study related with the people's life, the studies on the characteristics of the run-up wave due to the tsunami and the drifted body have been also performed.

As the studies on wave force due to run-up tsunami, Asakura et al. (2000) proposed a method of estimating tsunami force acting on the back-yard structure of the vertical sea wall through the laboratory experiments considering shallow water deformation. They also found that distribution of the wave pressure of the run-up wave acting on the structure can be estimated with the run-up wave level only in the absence of the structure, and this is expressed as a similar figure of hydrostatic pressure based on the run-up wave level. Ohmori et al. (2000) numerically reproduced the run-up wave level and fluid velocity on the vertical sea wall of Asakura et al.'s (2000) experimental results. As the results, it is known that the time variation of the wave force can be expressed with the modified Morison equation using wave level and fluid velocity.

For studies on behavior of drifted body and collision force due to tsunami, Matsutomi (1999) conducted small scale experiments in a channel and large scale ones in the air to obtain a practical formula for estimating the collision force on structures due to collision of driftwood. He also developed an analytical method based on the simplest elasto-plastic theory to examine the validity of the formula and characteristics of the collision force. In his study, it is pointed out that the coefficients of mass are 1.7 for surge and 1.9 for common flow in the formula for collision force. Additionally, Ikeno et al. (2001) investigated the behavior of the timber drifted by tsunami and its collision force on the vertical seawall. They pointed out that collision force can be obtained identically regardless of shapes of the drifted body if the momentum of a drifted body is identical. Moreover, Ikeno et al. (2003) discussed the collision forces of the drifted timbers due to run-up tsunami on the land. From these results, the wave force due to run-up tsunami is found to be larger than that due to non run-up tsunami. Haehnel

et al. (2004) conducted the laboratory experiments to estimate the maximum collision force of the woody debris on the structures in floodplain. They examined existing three representative approaches to estimate the maximum impact force, and found that all approaches can be summarized in one model which expressed in terms of the mass of the colliding body and the collision velocity.

Besides, studies on behavior of the vessel drifted by tsunamis have been also performed. Fujii et al. (2005b) carried out the laboratory experiments for behavior of an oil tanker under long period waves. They found out that there is phase difference between the motion of the wave level and the oil tanker furthermore the behavior of the oil tanker depends on degrees of an angle between wave and its initial directions. Ikeya et al. (2005, 2006) conducted similar laboratory experiments under the same conditions with Fujii et al.'s (2005b), and they measured the wave force acting on the vessel and the collision force of the vessel with the land structure as well as reproduced by numerical experiments. Additionally, Koike (2007) carried out the laboratory experiments for the behavior of small boats such as fishery boat and pleasure boat. His experiments showed a tendency that the drifting velocity of the boat more depends on its initial direction than its draft for large incident wave while depends on its draft for small incident wave.

A few studies on the behavior and collision of the container drifted by the run-up tsunami, the object in present study, have been carried out. Takagi (2005) conducted the laboratory experiments to understand behavior of a container drifted by run-up tsunami and its collision force on simplified container terminal model. As the results, the maximum wave level on the front surface of the fixed container is double as high as run-up wave level in the absence of the container, besides the collision force more depends on the water mass behind the container than the weight of the container. Mizutani et al. (2005, 2006) investigated the behavior of the container drifted by run-up tsunami and its collision force using scaled laboratory experiments. They pointed out the water mass (added mass) behind the drifted container plays an important role on the collision, and proposed a formula to estimate the collision force due to a drifted container considering the effect of the added mass. This estimation formula includes the volume of the added mass which is proportional to the collision time. In order to investigate the effect of the added mass on the collision force, Usami (2006) carried out the laboratory experiments with varying thickness of an acrylic resin plate (collided body), and he found that the effect of the added mass depends on the collision time due to varying stiffness of the collided body. Furthermore, Kumagai et al. (2007) reproduced Usami's (2005) experimental results using the Distinct Element Method (DEM). In the

Kumagai et al.'s study, not only the container but also the collided body were modeled by the distinct element in order to observe the effect of the stiffness and deformation of the collided body to the collision time, then it is known that the numerical method capable to estimate the same degree with the maximum collision force by the laboratory experiments. Arikawa et al (2006) conducted the large scale laboratory experiments for the drifted collision force of the steel container model scaled in 1/5 with the concrete collided body. They confirmed that the velocity of the drifted container has same value with the fluid velocity after it travels a certain distance, besides the collision force can be estimated using Arikawa et al (2003)'s estimation formula for the collision force between a wave dissipating block and a concrete wall in case of the small added mass due to high stiffness of the collided body. However, the effect of the added mass to the collision force was not discussed quantitatively. Nakamura et al (2006) investigated flow fields around a fixed container on the apron due to the run-up tsunami with three-dimensional numerical analysis. They clarified that the maximum wave pressure acting on the front surface of the container can be approximated by the distribution of hydrostatic pressure based on the maximum run-up wave level at the front surface of the container. Finally, Shiraishi (2006) investigated the collision force and time for the collision between the container and concrete pier using LS-DYNA, a code for nonlinear dynamic finite element analysis of structures in three dimensions. He pointed out that the collision time can be estimated by giving the physical properties of the material and the velocity of drifted container. However, it was not adequate for estimating accurate collision force and time because the interaction between the run-up wave and container was not considered in his simulation.

Although, the studies on the behavior of drifted container and collision force have been investigated as mentioned above, there have been some unclear matters. For example, quantitative estimation of the added mass for the collision force of the drifted container has not been carried out. Besides, the estimation of the collision force in full scale container has not conducted yet.

1.3 Study Objectives

As discussed above, there have been still many unknowns related to the behavior of the freight container drifted by run-up tsunami and its collision force, the present study therefore investigates the characteristics of the collision of drifted container. The specific targets of the present study are as follows:

- Behavior of container drifted by run-up tsunami
- Importance of added mass, which is the water mass behind the container contributing to collision of drifted container;
- Review of estimation formula for collision force of drifted container; and
- Coupling of drifting model and collision model.

When collision of a container drifted by run-up tsunami with a back-yard structure, not only weight of the container but also presence of water mass (added mass) behind the container may play an important role in the collision. In present study, behavior of the drifted container and the importance of the added mass are discussed through laboratory experiments.

Mizutani et al. (2005, 2006) proposed an estimation formula for the collision force of the container drifted by run-up tsunami, in which the formula is composed of a changing of momentum and an impulse with constant collision force. In present study, time variation of the collision force in the impulse is considered in the estimation formula to practical estimation of the collision force.

To simulate the collision of drifted container, LS-DYNA, a code for nonlinear dynamic finite element analysis of structures in three dimensions, is applied. For reproducing propagation of a tsunami wave by using LS-DYNA in which long period waves are employed, the calculation cost is extremely high. To reduce calculation cost, therefore, the present study carries out a coupling the collision model (LS-DYNA) with a drifting model using IB (Immerged Boundary) method. As employing the drifting model from wave generation to just before collision of container and LS-DYNA during collision of container, the drifting and collision phenomena are simulated. In this coupling, the relationship between velocity of drifted container and wave level behind the container from the drifting model is used as initial conditions in the collision model, LS-DYNA. From these work, the collision of drifted container can be reproduced in a practical manner.

As comparison with the results of LS-DYNA employing the relationship between velocity of drifted container and wave level behind the container by the drifting model, validity of the modified estimation formula is verified.

Analyses of the container collision using aforementioned coupling method are conducted in actual phenomenon. Then, the estimation formula for the collision force of the full scale drifted container is verified, a lot of database for estimating collision force using the estimation formula is offered as well. This database can be a helpful material

to estimate external force of the back-yard structure in design.

1.4 Contents

The present study investigates the behavior of a freight container on the apron drifted by run-up tsunami and the collision force with a back-yard structure by using estimation formula. The contents of this dissertation are summarized as follows.

In Chapter 2, the laboratory experiments scaled in 1/75 are conducted to understand the characteristics of the run-up tsunami and the behavior of the drifted container.

Long period waves, which have various wave heights and wave period, are employed as the tsunami. The container is modeled by an acrylic resin with considering the scale, and 40ft and 20ft containers are considered as a drifting body. To understand the behavior of drifted container in presence of a back-yard structure, a continuous wall, a squared structure and a column are employed as the back-yard structures. Importance of the added mass is confirmed through collisions with an acrylic resin plate as collided body in the absence of water and in the presence.

In Chapter 3, the estimation formula for the collision force of the drifted container expressed with a changing of momentum and an impulse proposed by Mizutani et al. (2005) is reviewed. In this dissertation, the author considers a time variation of the collision force in the impulse of the estimation formula, and investigates the exact maximum collision force of the drifted container.

In Chapter 4, previous to coupling between a drifting model using IB (Immerged Boundary) method and a collision model (LS-DYNA), governing equations and numerical schemes of the models are introduced. This IB method employs a body force proportional to a solid volume fraction for coupling the solid and fluid motions at the interface. In LS-DYNA, Arbitrary Lagrangian Eulerian (ALE) finite element method is used to solve fluid-structure interaction problems.

In Chapter 5, verifications of the drifting and collision models are carried out by comparison with the laboratory experiments, respectively, the coupling model is verified as well. The estimation formula modified in Chapter 3 is compared to the results of these coupling models, and its applicability is confirmed.

In Chapter 6, applicability of the modified estimation formula for the collision force of the drifted container to actual phenomenon is verified. Additionally for applying in plastic deformation on the container, the modified estimation formula is revised once more. Moreover, simplification of the estimation formula is carried out for practical utilization, thus it is expected that the collision force of the container drifted by the

run-up tsunami as the external force of the back-yard structure on a container terminal is easily obtained by using the estimation formula with the collision time.

Finally, in Chapter 7, the author presents the main conclusions as well as recommendations for future research.

The flow chart of the present dissertation is shown in Fig. 1.2.

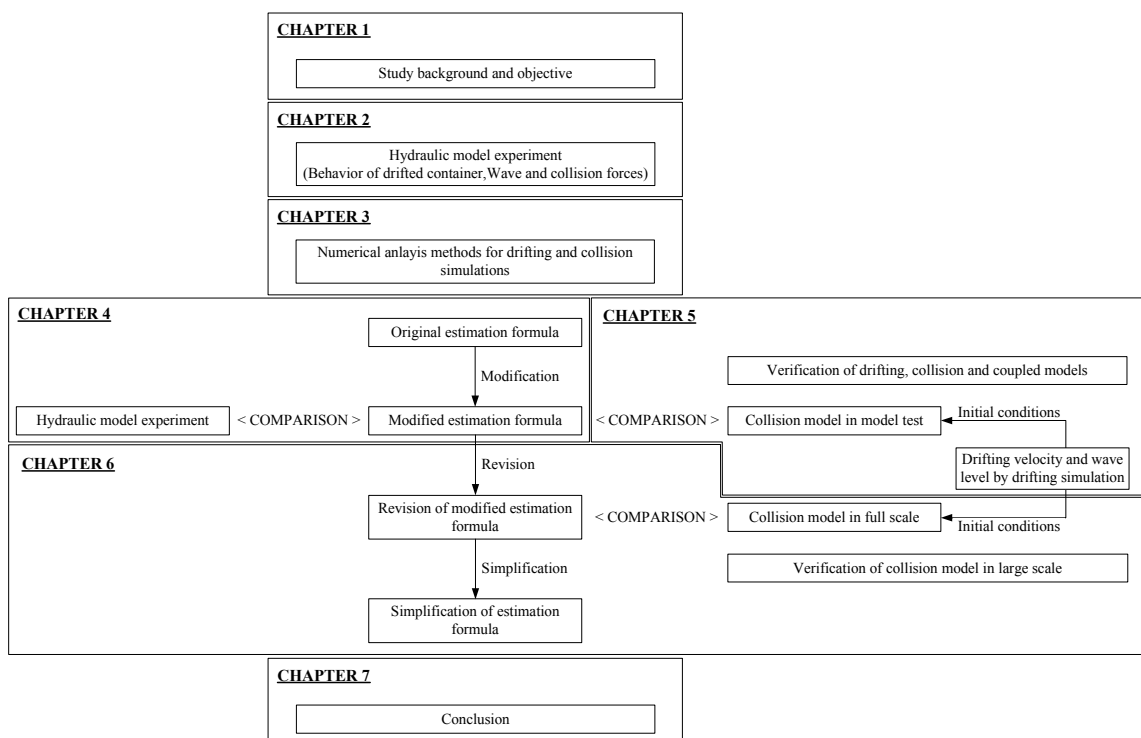


Fig. 1.2 Flow chart of the present dissertation

CHAPTER 2.

C H A R A C T E R I S T I C S O F R U N - U P T S U N A M I A N D B E H A V I O R O F D R I F T E D C O N T A I N E R

2.1 General

In tsunami disaster, not only direct damages by run-up wave but also indirect damages by drifted bodies may occur. Dangerousness of these drifted bodies had been reported by field surveys on 2004 Sumatra and 2006 Java tsunami disasters (Choi et al., 2005; Imamura et al., 2005; Tatsumi et al., 2007). Vessels, vehicles, lumbers, freight containers and destroyed debris can be the drifted body to trigger the indirect damages.

To predict the behavior of the drifted bodies, first of all, understanding of the characteristics of the run-up tsunami is an indispensable. Matsutomi and Iizuka (1998) proposed a simple estimation method for tsunami current velocity on land based on the energy conservation theorem considering energy loss. They pointed out that the run-up fluid velocity can be approximated as double the wave velocity of long period wave with the inundated depth ($u_m / \sqrt{g\eta_m} = 2$). The studies on the fluid velocity of run-up tsunami on the land such as aforementioned have not been implemented sufficiently, the author, therefore, clarifies the relationship between the fluid velocity and wave level on the land (apron in this study) using laboratory experiments. From these experiments, the characteristics of the run-up tsunami, which causes the drifting bodies, are discussed in this chapter.

Recently, because of a growing interest on the tsunami disaster including the indirect damages, studies on the behavior of the body drifted by the tsunami have been carried out actively. Fujii et al. (2005a, 2005b) investigated behavior of a vessel drifted by tsunami through laboratory experiments as well as numerical ones. In laboratory experiments, they found out that the behavior of the vessel is related with variation of the wave level and initial angle of the vessel. Besides, validity of the numerical method, which is a combination method of non-linear long wave theory and DEM (Distinct

Element Method) considering wave forces obtained from the Morison equation, was verified through comparison with the laboratory experiments. Fujii et al. (2007) proposed an evaluation method based on Fujii et al. (2005b) to predict the behavior of drifting bodies using the diffusion coefficient provided by laboratory experiments. Anno et al. (2007) considered the coefficient of drag force on cars as a function of each current angle into the aforementioned numerical method, and reported the application of that by comparing the drift motion with the experiment in the two-dimensional wave tank. Moreover, Matsutomi et al. (2007) presented a model for estimating the moving velocity of floating bodies. The model adopts the notion of the bore theory regarding the floating bodies as a hypothetical fluid, and takes account of the resistance due to the floating bodies piling up at the surge front of inundated flow.

Besides, various attempts to predict the damages by tsunami have been carried out, e.g. studies on relationship between the destruction of structures and surge front tsunami force (Arikawa et al., 2007) and on tsunami force acting on a structure group (Simamura et al., 2007) with laboratory experiments. However, there has not been an attempt to interpret behavior and velocity of a drifted body, a collision force of drifted body, and deformations of colliding and collided bodies, relationally yet. The present study examines on them and at first the characteristics of the run-up tsunami and the behaviors of the drifted bodies as varying back-yard structures are discussed experimentally.

2.2 Experimental Setups

Hydraulic model experiments were conducted on the basis of the Froude similarity law with a length ratio of 1/75 using a 30.0m long, 0.7m wide and 0.9m high wave flume with piston-type wave generator at the Department of Civil Engineering, Nagoya University. The maximum stroke of an equipped wave paddle is 1.50m, and hence the wave generator also has a capability of generating long-period waves.

The author placed a 0.57m high impermeable rigid apron with seaward slopes of 1/10 and 1/100 inside the wave flume as shown in Fig. 2.1, and water surface variations at W1-W13 and fluid velocities at W6-W13 were measured.

In the experiments, long period waves were employed as the incident wave, and the details are listed in Table 2.1, in which T is the time duration of wave generating plate moved from hindmost to forefront and H is the highest wave level above the still water level measured at W1.

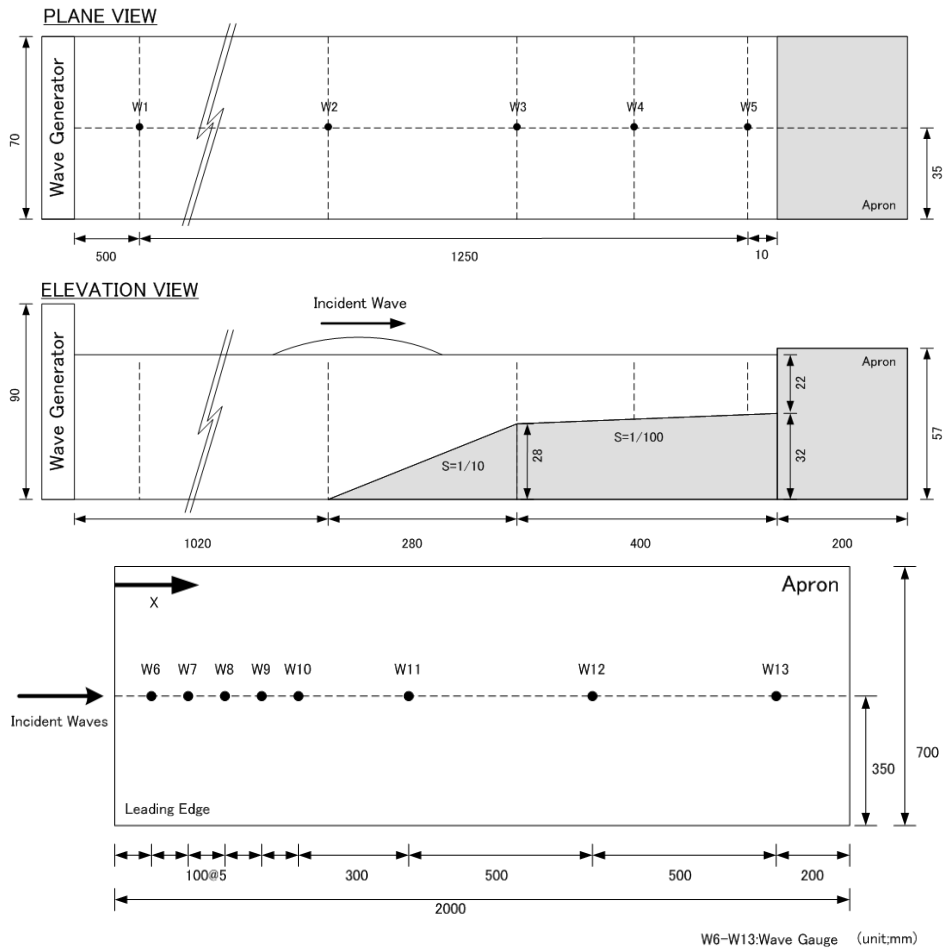


Fig. 2.1 Schematic figure of experimental setup and measuring points

Table 2.1 Incident wave conditions

	T [s]	H [cm]
Case 1	7.5	2.31
Case 2	7.5	3.11
Case 3	7.5	3.97
Case 4	7.5	5.20
Case 5	7.5	6.09
Case 6	10.0	2.13
Case 7	10.0	3.16
Case 8	10.0	3.97
Case 9	10.0	4.91
Case 10	15.0	2.81
Case 11	15.0	3.24

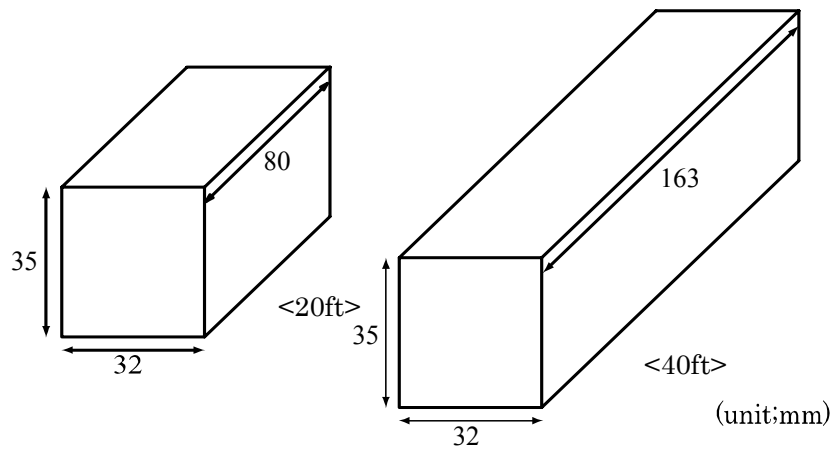
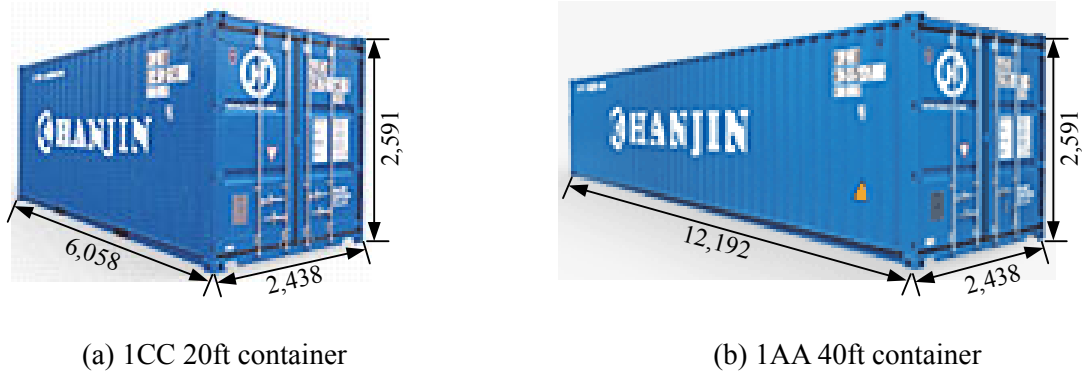


Fig. 2.2 Dimensions of scaled container models



(a) ICC 20ft container

(b) 1AA 40ft container

Fig. 2.3 Dimensions of ISO dry freight containers (unit: mm)

Source: <http://www.hanjin.com> and Japanese Industrial Standards Committee (1994)

Table 2.2 Mass and thickness of scaled container models

Class	20ft container			Class	40ft container		
	Mass [g]	Thickness [mm]	Note		Mass [g]	Thickness [mm]	Note
FT20G1	15.6	1.0		FT40G1	29.9	1.0	
FT20G2	23.2	1.0	Half-loaded	FT40G2	37.7	1.0	Half-loaded
FT20G3	30.6	2.0		FT40G3	42.2	1.5	
FT20G4	39.7	2.0		FT40G4	59.2	2.0	
FT20G5	52.2	4.0	Full-loaded	FT40G5	77.6	3.0	Full-loaded
FT20G6	83.8	4.0		FT40G6	132.7	3.0	

Dimensions of 20ft and 40ft container models scaled in 1/75 are illustrated in Fig. 2.2 and mass and thickness of the scaled containers used in the hydraulic model experiments are listed in Table 2.2. The container models are made with acrylic resin plates with thickness 1.0 to 4.0 mm. Because the thinnest acrylic plate used in the container models was 1.0 mm, it was incapable of reproducing the empty container. Scaled 40ft and 20ft containers are based on ISO 1AA 40ft and 1CC 20ft dry freight containers (Japanese industrial standards Committee, 1994), and the details of the ISO container are shown in Fig. 2.3.

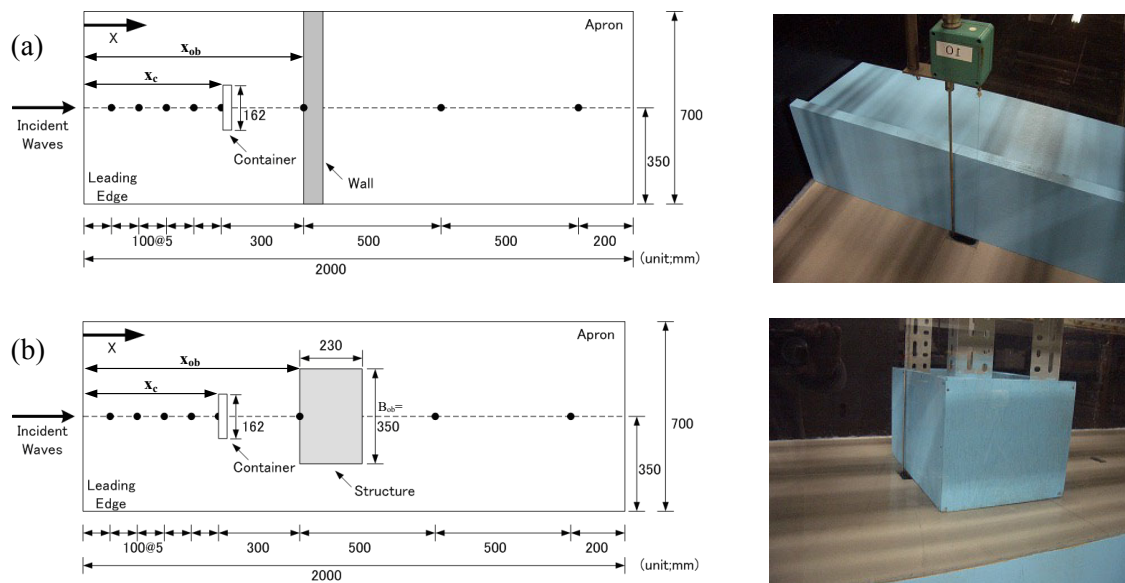


Fig. 2.4 Schematic figures of drifting container experiments (left) and back-yard structures (right): (a) continuous sea wall; (b) rectangular structure

To grasp the behavior of the drifted container as changing geometry of the back-yard structure, continuous sea wall and rectangular structure are employed as the back-yard structures. In Fig. 2.4, the left sides are the schematic figures and the right sides show the back-yard structure models used in the experiments. The containers and structures are placed at $x_c=50.5\text{cm}$ and $x_{ob}=80.5\text{cm}$ (see Fig. 2.4) from the edge of the apron as initial condition, respectively. To understand the mechanism of the container falling into the sea, the wave level fluctuation in front of the structure as well as the wave forces acting on the fixed container were measured. The right side in Fig. 2.4 (a) and Photo 2.1 show the wave level gauge placed at front of the continuous sea wall and the 6-component force transducers connected with the 40ft container, respectively. And just to confirm the possibility of the tsunami damage to inland area, effect of dimensions of



Photo 2.1 Container fixed by 6-component force transducers

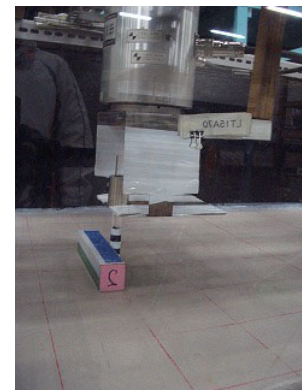
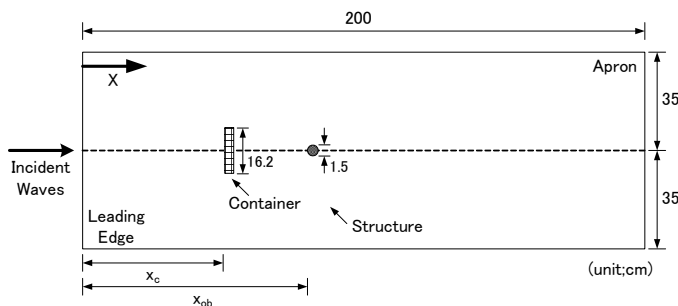


Fig. 2.5 Schematic figure of drifted container collision with column and the acrylic resin column connected with 6-component force transducers

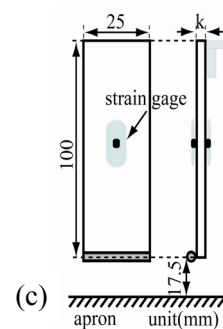
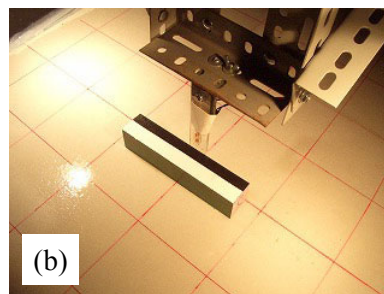
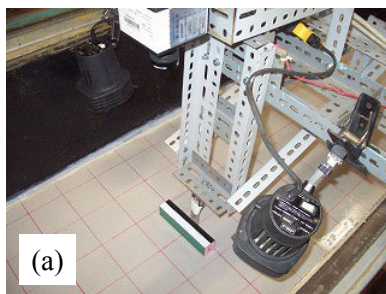


Fig. 2.6 Photo views of container model and acrylic resin plate as a collided body and schematic of the acrylic resin plate

the rectangular structure is not examined.

Besides, the collision tests of the drifted container in the company of water with a column are performed in order to understand the relationship between collision force and wave force. The schematic figure of the drifted container collision with the acrylic resin column and the column connected with 6-component force transducers are

illustrated in Fig. 2.5. In these laboratory experiments, the author concentrates on the growth of tsunami damage due to the presence of drifting body, and the effect of stiffness of collided body is discussed in full scale test (Chapter 6).

Furthermore, to grasp the effect of the water behind the container to the collision force, the author carried out the collision tests of the container with an acrylic resin plate in the presence of the water and in the absence. The high speed video camera was installed at the upper side of the apron and the calibrations were notched onto the apron in 10cm interval to observe the collision velocity of the container (Fig. 2.6 (a)). The upper part of the plate is fixed by angle bars strongly as shown in Fig. 2.6 (b). As shown in Fig. 2.6 (c), the lower part of the plate was placed at 17.5mm height and a wire was attached to concentrate the weight of the container. Additionally, the stiffness of the plate was considered by changing its thickness ($k=2$ and 4mm). Finally, measured displacement of the lower part of the plate was converted to the collision force via the strain gauge attached in the plate.

2.3 Experimental Results

2.3.1 Run-up wave level and fluid velocity

Fig. 2.6 shows the time variations of the wave level at each measurement point for Case 3 as the incident wave (see Table 2.1). The horizontal axis is the time since wave generating and the vertical axis is the wave level above the steel water level or apron height. The wave level at W5 where is ahead of the revetment shows a high value

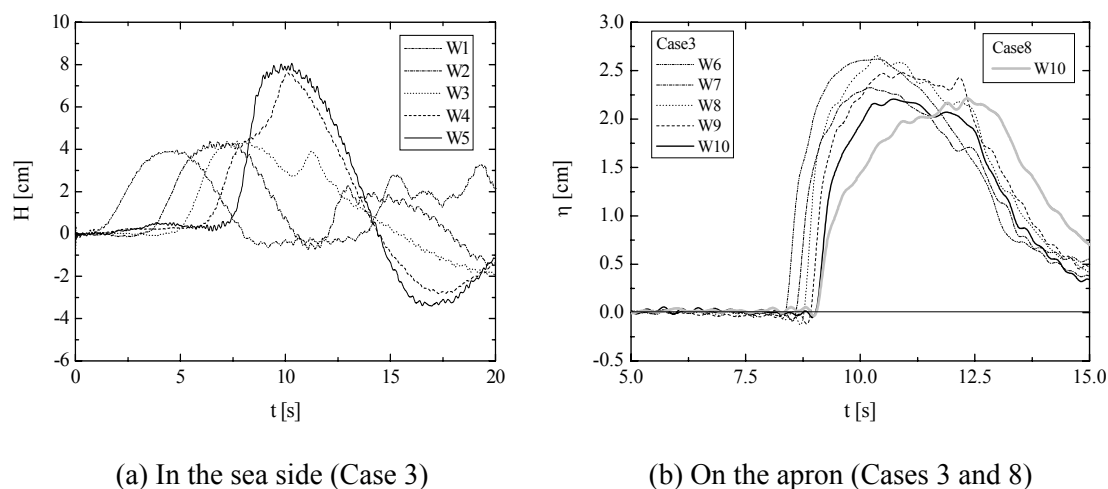


Fig. 2.7 Time variations of the wave level at each measurement point

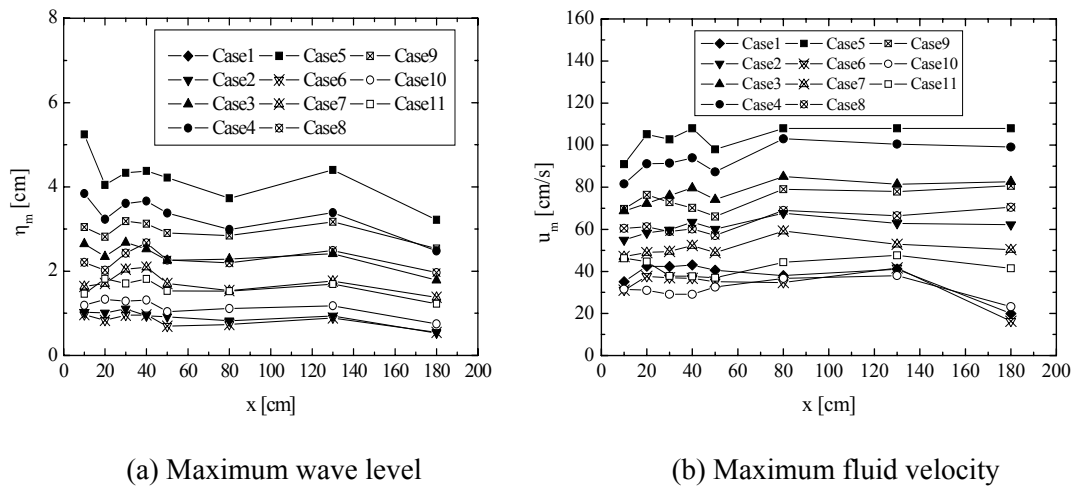


Fig. 2.8 Spatial distributions of the maximum wave level and maximum fluid velocity on the apron

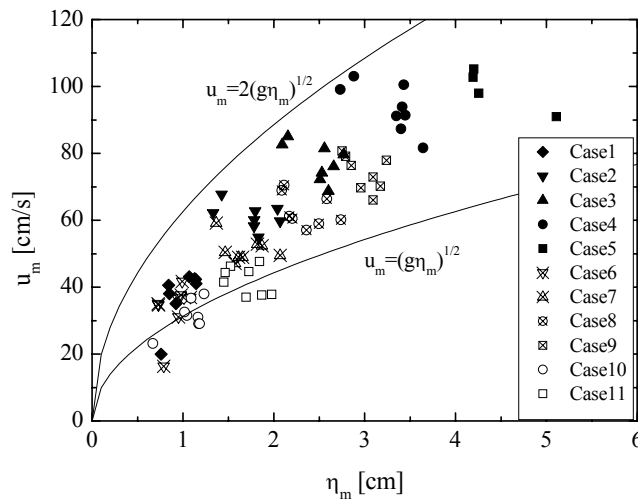


Fig. 2.9 Relationship between the maximum run-up wave level and maximum fluid velocity on the apron

related with other points because of standing wave due to presence of the revetment. In Fig. 2.7 (b), the run-up wave levels at W10 for relatively short (Case 3) and long period (Case 8) incident waves are compared. The maximum run-up wave levels for Cases 3 and 8 show the nearly same values, Case 8 which is the relatively long period, however, has longer duration to the maximum run-up wave level than Case 3. The author thinks that this phenomenon influences on the wave pressure and wave force acting on the container as well as the container drifting, and the present study concentrates on the container drifting mainly.

In Fig. 2.8, the maximum run-up wave levels and maximum fluid velocities on the apron for each wave condition are shown. The obvious fluctuation of the maximum run-up wave level is not found for the range of these experiments (Fig. 2.8 (a)), and the maximum fluid velocity also shows almost the same value on the apron except cases of the small fluid velocity (Case 1, 6 and 10) in Fig. 2.8 (b).

From the result of a little fluctuation for the maximum run-up wave level (η_m) and maximum fluid velocity (u_m) spatially, the author expects a certain relationship between them, and the relationship between them is shown in Fig. 2.9. In the figure, $u_m = 2.0\sqrt{g\eta_m}$ is the relationship in the dangerous condition by Matsutomi and Iizuka (1998), and the present result is satisfied with that. Besides, the Froude number expressed by the maximum run-up wave level (η_m) and maximum fluid velocity (u_m) in the present study is 1.5 approximately. This relationship will be investigated including drifting velocity of container in more detail in Chapter 5.

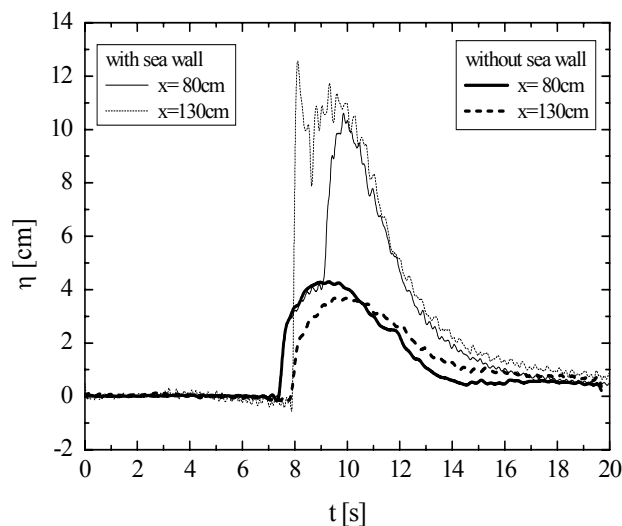
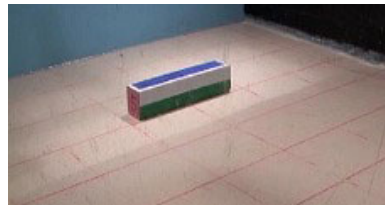


Fig. 2.10 Change of the wave level fluctuation due to the continuous sea wall (Case 5, $x_{ob}=130.5\text{cm}$)

2.3.2 Behavior of drifted container

The characteristics of the run-up wave level and fluid velocity on the apron were described in above subsection, and in this subsection, the behavior of the container drifted by the run-up wave with a back-yard structure is discussed. A continuous sea wall and a rectangular structure were employed as the back-yard structure, and FT40G2 and FT40G5 as listed in Table 2.2 were considered as the drifted container model.



(a) After 9.4s



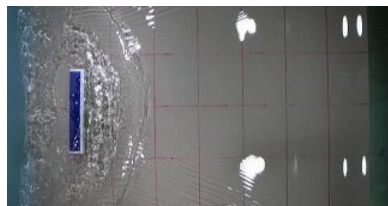
(b) After 9.6s



(c) After 9.8s



(d) After 10.0s



(e) After 10.2s



(f) After 10.4s

Photo 2.2 The behavior of drifted container in presence of the continuous sea wall (Case 4, FT40G5, $x_c=50.5\text{cm}$, $x_{ob}=80.5\text{cm}$)

2.3.2.1 Continuous sea wall as a back-yard structure

First of all, the influence of the run-up wave level fluctuation due to presence of the continuous sea wall is investigated. Fig. 2.10 shows the time variation of the wave level at $x=80$ and 130cm when the sea wall is installed at $x_{ob}=130.5\text{cm}$ or not. It is known that the wave level considered the sea wall is larger than that unconsidered, in which the values are almost three times, because of reflected waves from the sea wall. Besides, it also showed a similar tendency in the sea wall installed at $x_{ob}=80.5\text{cm}$. The behavior of the drifted container in presence of the sea wall was obviously different from in absence of that. The drifting behavior of the FT40G5 container placed at $x_c=50.5\text{cm}$ initially due to presence of the continuous sea wall at $x_{ob}=80.5\text{cm}$ shows in Photo 2.2. The left and right photos are video images taken from upside and inclined side, respectively. Some parts of the run-up waves progressed (Photo 2.2 (a)) on the apron collides with the container, and the container drifting is commenced (Photo 2.2 (b)). On the other hand, other parts of the run-up waves passed over the container sides reach to the sea wall before the container, while the other parts round into the landside of the container (Photos 2.2 (c) and (d)). The container is, then, decelerated due to the water rounded into the container and reflected waves from the sea wall (Photo 2.2 (e)). These rounded water and reflected waves play a buffer role between the container and sea wall, and interrupt the collision (Photo 2.2 (f)). A large number of these cases were confirmed in the experiments, while a few number of colliding with the sea wall. It is inferred that a container drifted by run-up tsunami rarely collides with the continuous structures. Furthermore some phenomena were found out through the laboratory experiments as following.



(a) Case of falling down to the sea (Case 8) (b) Case of drifted to the seaside (Case 3)

Photo 2.3 Examples of the behavior of the drifted container due to the reflected waves
(FT40G2, $x_c=50.5\text{cm}$, $x_{ob}=80.5\text{cm}$)

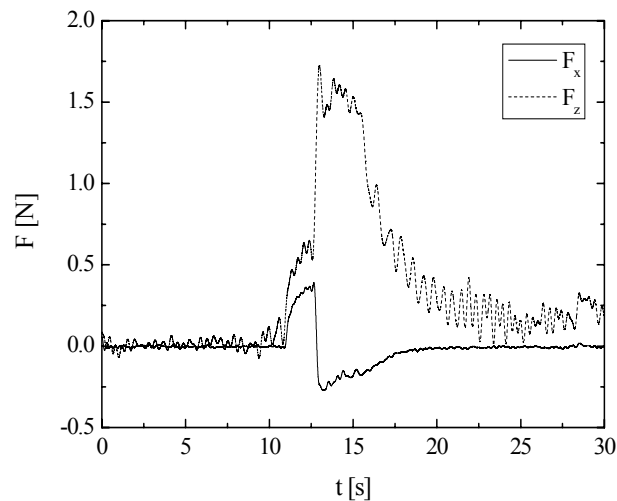


Fig. 2.11 Wave forces acting on the container (Case 7, $x_c=50.5\text{cm}$, $x_{ob}=80.5\text{cm}$)

It was confirmed that the drifted container, which was not collided due to the effect of the reflected waves, shifts the direction to the seaward or revolves on its axis in the complex wave fields. The container was then either stopped on the apron or fallen down to the sea (Photo 2.3 (a)). These phenomena were occurred mainly for the sea wall ($x_{ob}=80.5\text{cm}$) closed to the container and relatively light containers (FT40G2). Besides, when the incident wave height was large, the container was floated completely due to the reflected waves, and drifted to the seaward then fallen (Photo 2.3 (b)). These phenomena such as container falling down to the sea and floating had been occurred on Tokachi-oki earthquake in 2003, and hindered disaster repair works in the seaside (Tomita et al. 2004). It is, therefore, necessary to investigate the countermeasures for preventing the container falling down to the sea, especially a sea route or a berth.

So far, researchers have been concentrated on the collision force of the drifted container with back-yard structures (e.g., Kumagai et al., 2007; Mizutani et al., 2006), however the container drifting to the seaward should be also investigated because of aforementioned teachings. Fig. 2.11 shows the time variation the wave force (F_x ; inland direction is the positive) and buoyant force (F_z ; upper direction is the positive) acting on the fixed 40ft container (refer to Photo 2.1). The run-up wave collides to the container on $t=11.0$ (s), and the wave and buoyant forces are increased together. The container, however, is not moved because the wave force smaller than the maximum of static friction force. After that, on $t=12.5$ (s), the reflected waves from the sea wall acts on the container, in the other hand, the direction of the horizontal wave force acting on the container is shifted to the seaward. And the buoyant force is rapidly increased since the wave levels around the container rose. In the experiment, the container was fixed by 6-component force transducers. In the actual condition, while increasing the buoyant

force, the container is floated then drifting is commenced due to the wave force toward to the seaside. Therefore, the effect of the reflected waves from the back-yard structures is important factor to establishing the countermeasure for the drifting prevention of containers.

2.3.2.2 Rectangular structures as a back-yard structure

The behavior of the drifted container on the apron in the presence of a rectangular structure ($B_{ob}=35.0\text{cm}$ or 23.0cm) is discussed. The run-up wave level fluctuation at front of the rectangular structure showed a similar tendency with that of the continuous sea wall. It was, however, confirmed that the wave level was smaller than that with the continuous sea wall because of over passing flow toward to inland. The behaviors of the container were divided into three types due to kinds of containers, incident wave conditions and width of the structure.

First of them is that the container drifts away to the rear side of the structure. In this case as shown in Photo 2.3, the run-up waves round into the sides of the drifting container (Photo 2.3 (a)) and are reflected from the structure (Photo 2.3 (b)), hence the container do not collide to that (Photo 2.3 (c)). At that time, the pressure on sides of the structure decreases because of the presence of the run-up waves passing through the structure, and drifting of the container commences toward the side (Photo 2.3 (d)), after all, the container is swept away by the run-up waves to the rear of the structure (Photo 2.3 (e) and (f)). As the results, it is pointed out that the damages due to the drifted bodies are able to occur in not only the coastal area but also inland area.

Secondary case is that the container is stopped in front of the structure after over passing the run-up waves as shown in Photo 2.4. In the photo, the container does not collide with the structure because of the run-up waves rounding the container and reflected waves, while it approaches slowly to the structure then is stopped in front of that because of relatively small volume (Photo 2.4 (b) and (c)) of the water between the container and the structure. These phenomena were found for wave conditions of the small run-up wave level however frequency in occurrence was low. While the structure was considered as an impermeable one in these experiments, representative structure as the rectangular structure, a building, in actual condition has many windows and entrances. And it is expected that the run-up waves collide the building, and intrudes into that. It is inferred that the water volume between the container and structure in actual condition is smaller than that in the experiments. In actual condition, hence the container collision with structure could be occurred more easily.



(a) After 0.3s



(b) After 1.1s



(c) After 1.5s



(d) After 2.6s

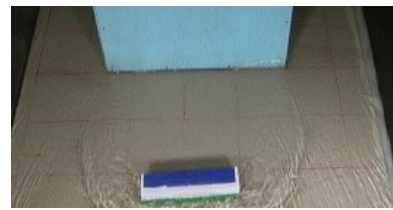


(e) After 3.0s



(f) After 3.4s

Photo 2.3 Behavior of the container in presence of the rectangular structure - drifted away (Case 4, FT40G5, $x_c=50.5\text{cm}$, $x_{ob}=80.5\text{cm}$, $B_{ob}=35.0\text{cm}$)



(a) After 0.5s



(b) After 1.2s



(c) After 1.4s



(d) After 2.0s



(e) After 3.0s



(f) After 4.0s

Photo 2.4 Behavior of the container in presence of the rectangular structure - stopped (Case 3, FT40G2, $x_c=50.5\text{cm}$, $x_{ob}=80.5\text{cm}$, $B_{ob}=35.0\text{cm}$)

Lastly, it is the case that the container collides with the structure. In the experiments, this phenomenon was found for the relatively small width structure ($B_{ob}=23.0\text{cm}$) as well as small period and small run-up wave level, mainly. Because of the relatively small rounding water around the container and reflected waves, it is inferred that the influence of the water between the container and structure as a buffer is a little.

2.3.3 Collision and wave forces

In this subsection, the collision force of a drifted container with a column and the wave force as shown in Fig. 2.5 are discussed. Examples of the time variations of the collision and wave forces are depicted in Fig. 2.12 when the drifted container is stopped at front of the column after collision, in which F_x and F_y represent the collision force and perpendicular force. The enormous force, which is a collision force, acts immediately after the collision ($t=10$ (s)) and is approximately double of the force during $t=10-13$ (s), which is a wave force acting on the stopped container. Moreover, this wave force in presence of the container ($B_c=16.3\text{cm}$) is approximately ten times as large as the wave

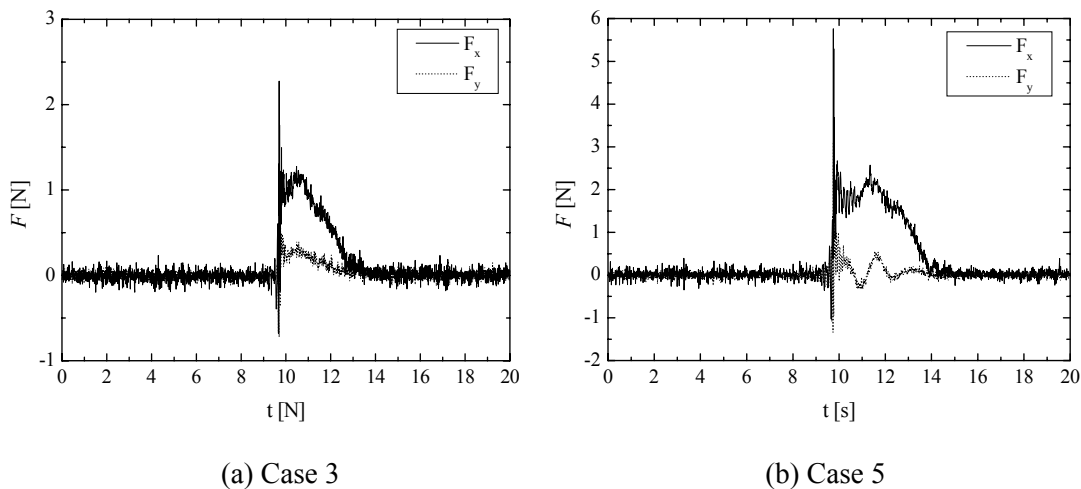


Fig. 2.12 Time variation of the collision and wave forces acting on the column (FT40G2, $x_c=50.5\text{cm}$, $x_{ob}=80\text{cm}$)

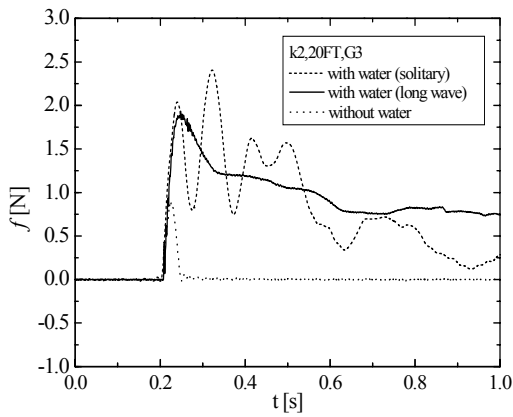
Table 2.3 Maximum forces acting on the column (unit; N)

	In absence of container (wave force)	Oblique collision (collision force)	Reasonable collision (collision force)
Case 3	0.1	1.3	2.4
Case 5	0.2	2.4	5.7

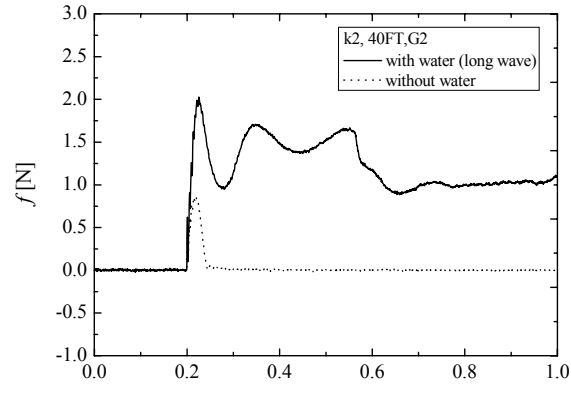
force acting on the column in absence of the container (Table 2.3). It is known that although it is the slow fluid velocity or small run-up wave level, the wave force acting on the column can be increased due to the presence of the drifting body (container). Besides, in not only the reasonable (longitudinal direction of the container is perpendicular to its translational direction at the moment of collision) collision as mentioned above but also the oblique ones, the large collision force was found (Table 2.3). From the results, it is expected that tsunami damages are extended due to the bodies drifted by run-up tsunami. Therefore, the prefer countermeasures should be made up for the potential damages by the drifting bodies.

2.3.4 Importance of added mass

The influence of presence of the water behind the container on the collision force of the drifted container is discussed. The experiments were conducted in presence of water and in absence, respectively, and the other experimental conditions are identical as shown in Fig. 2.6. The collision forces in same degree of the collision velocity for same kind of container are compared, and the examples are represented in Figs. 2.13 and 2.14. For presence of the water, almost same height long period and solitary waves were employed as the incident waves and are described as “with water (long wave)” and “with water (solitary)”, respectively. It is found that the collision force is changed due to the variation of the stiffness of the plate as the collided body, e.g. the collision force is small whereas collision time is long for the relatively thin plate, k2 (2mm). Besides, it is known that the magnitude and the duration of the collision force in presence of water (with water) is larger than in absence of that (without water) in no relation with magnitude of the stiffness of the plate. As a cause of the difference, it can be given that the water mass behind the container plays as an added mass during the container collision with the plate. Therefore, the effect of the added mass is remarkable for the thin plate (k2) with the long collision time. In order to evaluate the effect of the added mass which is a water mass behind the container contributing the maximum collision force, the quantitative analysis should be carried out. As the representative study on it, Mizutani et al. (2005) proposed an estimation formula for the collision force of the drifted container. The present study examines and modifies the estimation formula proposed by Mizutani et al. (2005), and then performs the numerical fluid structure interaction (FSI) analyses to confirm applicability of the estimation formula.

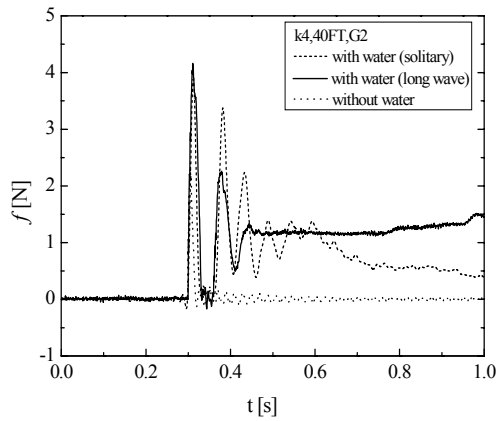


(a) FT20G3

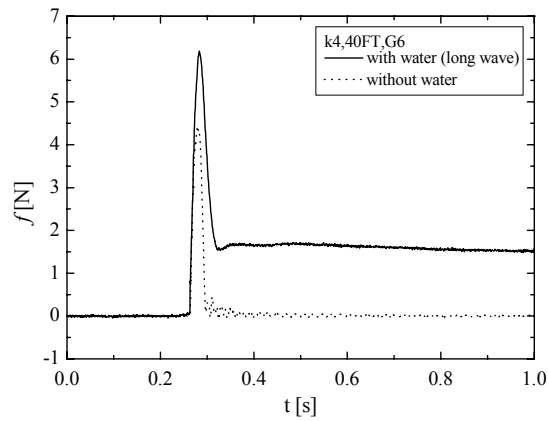


(b) FT40G2

Fig. 2.13 Time variations of the collision force (plate; k2)



(a) FT40G2



(b) FT40G6

Fig. 2.14 Time variations of the collision force (plate; k4)

2.4 Remarks

To predict the behavior of the drifted bodies that trigger the secondary tsunami damages, first of all, understanding of the characteristics of the run-up tsunami and the behavior of drifted bodies is an indispensable. In this chapter, the author experimentally examined the characteristics of the run-up tsunami and the behaviors of the drifted bodies as varying back-yard structures, and described the relationship between wave force and collision force due to the run-up tsunami and the importance of the added mass.

As a result, the author obtained the following results:

1. The waves with approximately 1.5 in the Froude number which is expressed by the maximum run-up wave level (η_m) and maximum fluid velocity (u_m) were employed for wave run-up on the apron and behavior of the drifted container, and this relationship is satisfied with Matsutomi and Iizuka's results (1998).
2. For drifting behavior the container in presence of the continuous sea wall, the container was either stopped on the apron or fallen down to the sea due to the reflected waves from the continuous sea wall. Besides in presence of the rectangular structure, most container models were drifts away to the rear side of the structure due to the flows on the sides of the structure. It was pointed out that the damages due to the drifted bodies are able to occur in not only the coastal area but also inland area.
3. The wave force acting on the column was increased by the presence of the drifting body in spite of slow fluid velocity and small run-up wave level. Thus it is expected that tsunami damages are extended due to the bodies drifted by run-up tsunami, and the proper countermeasures on the drifting bodies should be established.
4. The magnitude and the duration of the collision force in presence of the water behind container were larger than those in absence of the water. In order to evaluate the effect of the added mass which is water mass behind the container contributing the maximum collision force, this study examined and modified the estimation formula for collision force of drifted container proposed by Mizutani et al. (2005).

CHAPTER 3

REVIEW OF ESTIMATION FORMULA FOR COLLISION FORCE OF DRIFTED CONTAINER

3.1 General

It is known that estimating the collision force of the drifted bodies in company with the run-up wave is important to understand the damages due to the run-up tsunami. If it is possible to estimate the drifting collision force by using the estimation formula, it may be a powerful tool in the research field of tsunami disaster. As the related studies regarding the estimating method for the collision force of drifted body due to run-up tsunami, Matsutomi (1999) developed an analytical method for estimating collision force of driftwood based on the simplest elasto-plastic theory and examined characteristics of the collision force and time. Haehnel et al. (2004) examined existing three representative approaches to estimate the maximum impact force of the wood debris on the structure in the floodplain, and found that all approaches can be summarized in one model which expressed in terms of the mass of the colliding body and collision velocity. Mizutani et al. (2005) proposed a formula to estimate the collision force of a drifted container considering the effect of the water mass behind of the container based on relationship between impulse and momentum. Besides, Ikeya et al. (2006) investigated the collision force of the drifted vessel as using equation of motion including inertia, viscous damping and reaction forces.

Among aforementioned estimation formulae for the collision force of drifted body, the present study reviews and modifies the formula proposed by Mizutani et al. (2005) for the collision of drifted container. They pointed out that the added mass behind the drifted container plays an important role on the collision force and is depended on the collision time, in which the added mass denotes the water mass contributing on the maximum collision force. As the related studies on the added mass, Minorsky (1959), Motora et al. (1971) and Petersen and Pedersen (1981) proposed the added mass coefficient for motion of vessel via a series of model tests and hydrodynamic analyses. The researches on the added mass of the floe's collision, besides, reported in "Ice

mechanics risks to offshore structures” (Sanderson, 1988). In the report, it is described that the added mass is caused by the changes that are necessary to the surrounding flow field as the body’s motion alters, and it can be expressed simply as an additional mass using water depth and draft which is added to the body’s inertial mass. Ikeya and Tanaka (2003) estimated the added mass coefficient according to changing conditions (lateral and longitudinal column, square pillar and sphere) of the drifted bodies by the laboratory experiments.

However, the studies related to the added mass in the collision of container have not been conducted. The present study examines thoroughly on it with the estimation formula by Mizutani et al. (2005). Furthermore, their formula is modified as considering time variation of collision force, and then improvement of the modified formula is described through the comparison with the original formula.

3.2 Review of Estimation Formula

Mizutani et al. (2005) proposed the estimation formula for the collision force of the container drifted by run-up tsunami based on impulse and momentum as follows:

$$f_{xm}\Delta t = (m_c + \alpha\rho_w\eta_m B_c V_x \Delta t)V_x \quad (3.1)$$

$$f_{xm} = m_c V_x / \Delta t + \alpha\rho_w\eta_m B_c V_x^2 \quad (3.2)$$

where f_{xm} is the maximum collision force; Δt is the collision time which is defined as the duration from commencement of the collision to the maximum collision force; m_c is the mass of container; ρ_w is the water density; η_m is the maximum wave level on the apron in absence of the container; α is the coefficient of run-up in presence of the fixed container ($\alpha = \eta_{mx} / \eta_m$; η_{mx} is the maximum wave level in front of the fixed container on the apron); B_c is the length of the container in perpendicular direction of the wave propagation; and V_x is the drifted velocity of the container just before the collision. The concept of this formula is that the changing amount of momentum during the collision is equal to the impulse, and it is known that in Eq. (3.1) which is composed of the impulse on the left member and momentums of the container and the added mass on the right member. Besides, the fluid velocity of the water behind the container for the collision is approximated to the drifted velocity of the container by assuming that the container and run-up wave behind the container move together. Fig. 3.1 shows the

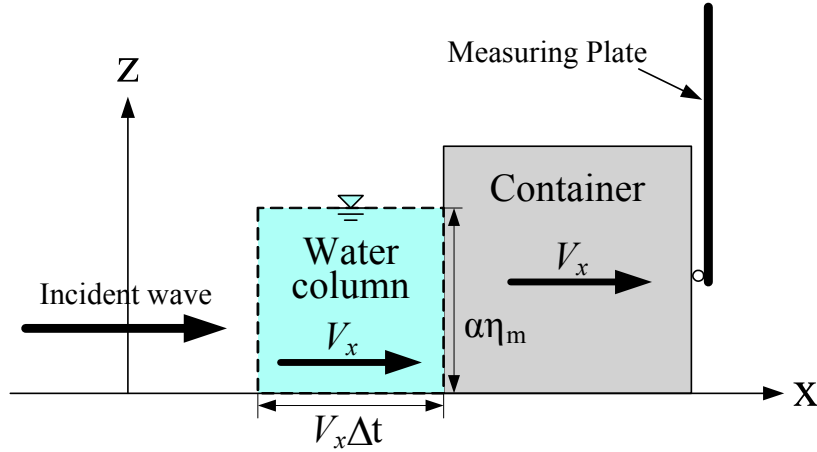


Fig. 3.1 Concept of the added mass

concept of the added mass employed in the estimation formula. It is known that the shape of the added mass is considered as a hexahedron with $\alpha\eta_m$ in height, $V_x\Delta t$ in length and B_c in width from Eq. (3.1) and Fig. 3.1. Mizutani et al. (2005) used a flexible acrylic resin plate as the collided body to estimate the load easily, in which the plate behaves such as the cantilever which the upper part is fixed. The collision force which is concentrated at the end of the plate as shown in Fig. 3.1 is calculated with the displacement of the end and the bending stiffness of the plate. Hence the drifted velocity (V_x) becomes zero when the collision force reaches peak value (correspond to maximum displacement of the end of the plate).

The author realized that the formula considers the impulse with the constant maximum collision force, therefore carried out some modification. In present study, the time variation of the collision force is considered in the impulse instead of the constant collision force of the original formula. Hereafter, it is called as the constant impulse and the integrated impulse, respectively. The modified estimation formula can be written as follow:

$$\int_{t_1}^{t_2} f_x(t)dt = (m_c + \rho_w \eta B_c V_x \Delta t) V_x \quad (3.3)$$

where $\Delta t = t_2 - t_1$; t_1 is the moment of the collision commencement; t_2 is the moment of the maximum collision force; and the wave level behind drifted container (η) is adopted instead of $\alpha\eta_m$ because the run-up coefficient (α) indicates the effect of the inertia force after collision. The concepts of the constant impulse in the original formula and the integrated impulse in the modified one are illustrated in Fig. 3.2. Ratio of the integrated impulse to the constant one can be expressed as Eq. (3.4). Substituting

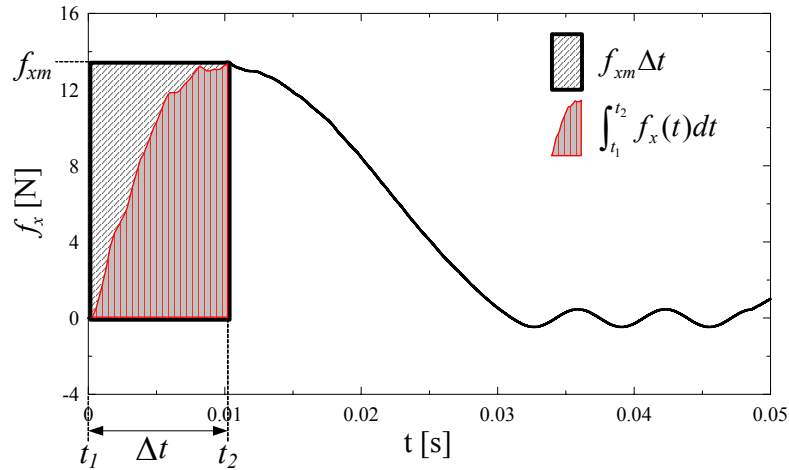


Fig. 3.2 Constant impulse in the original formula and integrated impulse in the modified formula

Eq. (3.4) to Eq. (3.3), Eq. (3.3) can be written as Eq. (3.5). Finally, the modified estimation formula for the collision force of the drifted container considering the time variation of the collision force has been revised as in Eq. (3.6). Additionally β will be called as the integration coefficient hereafter.

$$\frac{1}{\beta} = \frac{\int_{t_1}^{t_2} f_x(t) dt}{f_{xm} \Delta t} \quad (3.4)$$

$$\frac{1}{\beta} f_{xm} \Delta t = (m_c + \rho_w \eta B_c V_x \Delta t) V_x \quad (3.5)$$

$$f_{xm} = \beta (m_c V_x / \Delta t + \rho_w \eta B_c V_x^2) \quad (3.6)$$

3.3 Improvement of Estimation Formula

To verify the validity of aforementioned estimation formula modified by considering time variation on the collision force, the author carried out the comparison with the hydraulic model experiments. The experiments were conducted on the basis of the Froude similarity law with a length ratio of 1/75 using the wave flume at the Department of Civil Engineering, Nagoya University, in identical with Section 2.2. Fig. 3.3 shows the schematic figure employed in the collision experiments of the container drifted by run-up waves. Seaward slopes of 1/10 and 1/100 and 0.48m high

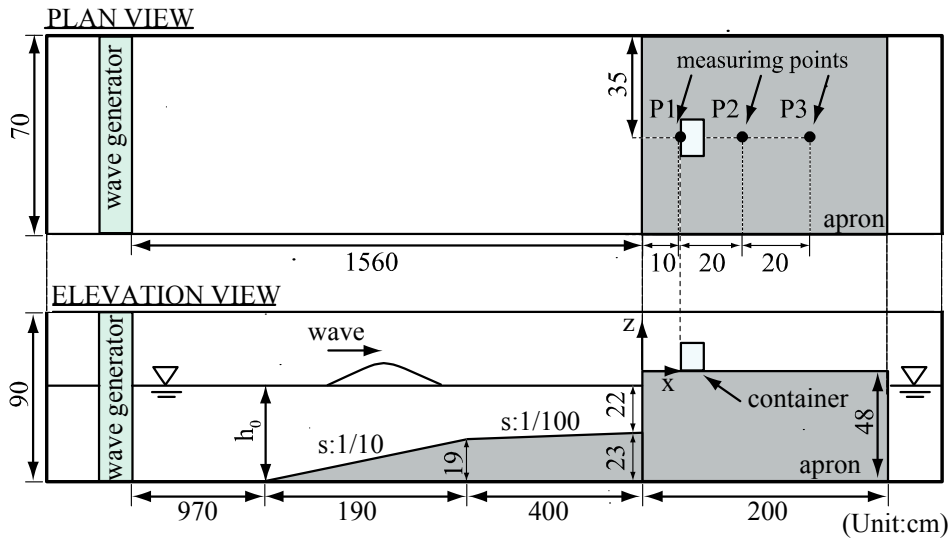


Fig. 3.3 Schematic figure of experimental setup and measuring points

Table 3.1 Incident wave conditions

Run	Wave	h_0 [cm]	T [s]	H [cm]
Case 1	L	45.0	12.5	2.8
Case 2	L	45.0	10.0	3.5
Case 3	L	45.0	10.0	3.1
Case 4	L	45.0	7.5	2.6
Case 5	S	45.0		2.8
Case 6	S	45.0		3.5

※ L: Long period wave, S: Solitary wave

impermeable rigid apron were placed inside the wave flume. P1, P2 and P3 represent the measurement points for wave fluctuations, fluid velocities and collision forces, and the collision forces of the container at P2 drifted from P1 are representatively discussed for validity of the modified estimation formula. The acrylic resin containers and plates were used as the colliding and collided bodies identically with Section 2.2. The incident waves were employed four long period waves and two solitary waves, and the details are listed in Table 3.1, in which h_0 is the water depth; T is the time duration of wave generating plate moved from hindmost to forefront; and H is the maximum wave level above still water level measured at 5.0m away from wave generator.

The collision tests were conducted with various weighted 40ft container models (refer to Fig. 2.2 and Table 2.2) and three kinds acrylic resin plates which are k2, k3 and k4 (2, 3 and 4mm in thickness). Among the experimental results, the author used only the reasonable collisions between the container and plate in the present dissertation, in which inclined and eccentric collisions were not considered. The comparisons of the maximum collision forces from the experiments (horizontal axis) and formulae (vertical

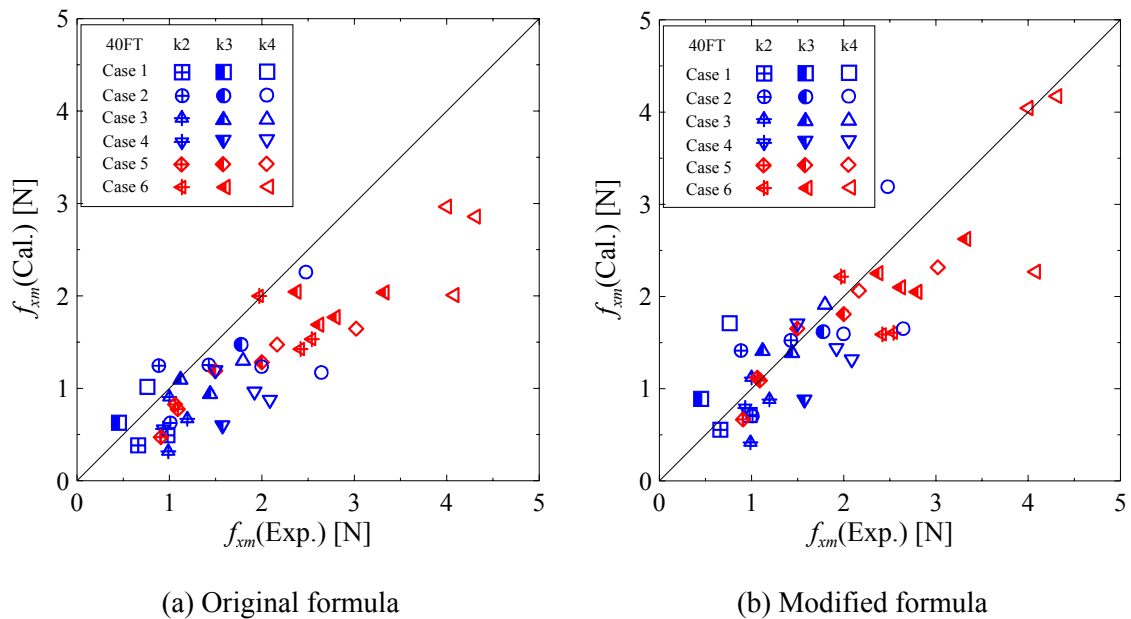


Fig. 3.4 Comparisons of the maximum collision forces by the laboratory experiments and estimation formulae

axis) are showed in Fig. 3.4, and left and right sides represent the comparisons with the results by the original formula and modified one, respectively. From the figure, it is confirmed that the results from the modified formula agree with those from the experiments than the original formula. In the right side, however, it is found that unevenness is relatively larger than the left side. The author concluded that the cause is the integration coefficient (β). The modified estimation formula depends on the integration coefficient, which is very sensitive to the colliding conditions. However, the modified formula (right side) is more reasonable than the original one (left side) in the safety aspects. The modified estimation formula is improved from the original one, and the validity for various conditions of the modified formula is confirmed through the numerical model experiments in next chapters.

3.4 Remarks

The estimation formula for the collision force of the drifted container by Mizutani et al. (2005) was reviewed to estimate more exact drifting collision force in this chapter.

As a result, the author obtained the following results:

1. The existing estimation formula which uses the constant maximum collision force in term of impulse was modified by considering time variation of collision force.

-
2. In term of comparison with the estimation formulae and experimental results, it was confirmed that the modified estimation formula agree with the experiments than the original estimation formula.

CHAPTER 4

N

UMERICAL MODEL

4.1 General

To confirm the validity of the modified estimation formula for the collision force of the drifted container for various conditions, comparisons with not only laboratory experiments but also numerical ones are performed. On estimating the collision force of drifted container through the numerical experiments, the non-linear finite element code, LS-DYNA, is used in the present study.

Since the first finite element model was developed by Turner et al. (1956), many commercial models have been introduced. Most of finite element models are used in research fields such as construction analysis, vehicle collision, and falling electronic equipment. As the representative models, SAP, MSC.NASTRAN, MSC.DYTRAN, ABAQUS, and LS-DYNA can be given. On the other hand, there are not so many models to capable of the fluid-structure interaction analysis. The LS-DYNA is a representative finite element model to enable the fluid-structure interaction analysis. In the present study, ALE (Arbitrary Lagrangian Eulerian) method in the LS-DYNA is used to analyze the container collision under fluid-structure interaction. The most important weakness of ALE method is the high calculation load, in which the calculation is divided the Lagrangian step for the analysis of structure and the Eulerian step for the analysis of fluid. From this point, the drifting model based on Immersed Boundary (IB) method for the container drifting is coupled with the LS-DYNA. By employing drifting model from wave generation to just before the collision of container and the collision model (LS-DYNA) during the collision, the calculation load can be reduced. The governing equations and calculation schemes of the drifting and collision models are described next sections.

4.2 Drifting Model

Recently, the researchers in a field of coastal engineering have been concentrated on the fluid-structure interaction problem as advances in computer. As the representative studies on it, Kawasaki et al. (2005a, 2005b) developed two- and three- dimensional multiphase numerical models using a CIP (Constrained Interpolation Profile) method and an extended SMAC (Simplified Marker And Cell) method in order to discuss complicated hydraulic phenomena, and improved the fluid-structure interaction analysis such as freely falling of a rigid body onto a still water surface, behavior of a container drifted by a surge, and behavior of floating bodies composed Lagrangian particles (Kawasaki et al., 2007; Kawasaki and Ogiso, 2008). Kumagai et al. (2006, 2007, 2008) investigated behavior of a drifted container using DEM (Distinct Element Method) and discussed on the applicability of the model to the field through comparisons with hydraulic model and field experiments. Ushijima et al. (2003) developed a computational method, MICS (Multiphase Incompressible flow solver with Collocated grid System), to predict the particle drag coefficients and wake flows, and applied to a falling particle near a side wall and non-uniform particles moving on the inclined bottom surface. Ushijima et al. (2006, 2008, 2009) then extended the MICS to analysis of interactions between objects and free-surface flows, and investigated the movements of spheres, arbitrarily-shaped objects and driftwoods due to three-dimensional free-surface flows. Besides Yoneyama et al. (2008) proposed a numerical analysis method to predict the behavior of drifting object in a tsunami inundation. This code using the FAVOR (Fractional Area Volume Obstacle Representation) method to set the boundary between a fluid and an obstacle and the VOF (Volume Of Fluid) method for representing a free surface was applied to the object drifted by a run-up tsunami.

In recent years, IB (Immerged Boundary) method which was firstly used in a field of medical science (e.g., Peskin, 1977) has been applied in a field of computational physics (e.g., Ishii et al., 2006; Choi et al., 2007). Lee and Mizutani (2007) applied Lima E Silva et al.'s (2003) IB method considering complex geometry on a standard regular Cartesian grid in a field of coastal engineering, and investigated the wave force acting on a horizontal circular cylinder. This IB method considers the interfacial force on a finite number of Lagrangian points which are distributed over the solid-fluid interface as the external force on the Eulerian grid, which is named Physical Virtual model. There is, however, a difficulty to extend to three-dimensional analysis because of increasing Lagrangian points.

From this point, the author refers an IB method of body force type proposed by Yuki

et al. (2007), which the object is represented as the solid volumetric fraction in each cell, to the fluid-structure interaction analysis. The behavior of a container drifted by run-up tsunami is examined as incorporating in Nakamura et al.'s (2008) three-dimensional numerical wave flume based on MARS (Multi-interface Advention and Reconstruction Solver).

4.2.1 Governing equations

Golshani et al. (2003) developed a three-dimensional fully non-linear numerical model capable of reproducing wave-induced flow fields inside and around a vertical permeable structure based on the VOF (Volume Of Fluid) method (Hirt and Nichols, 1981). Hur et al. (2007), then, added the molecular viscosity terms omitted by Golshani et al. (2003) to improve the computational accuracy. Nakamura et al. (2008), furthermore, additionally improved the numerical model of Hur et al. (2007). They added surface tension effect based on the CSF (Continuum Surface Force) model (Brackbill et al., 1992) and eddy viscosity effect based on the DTM (Dynamic Two-parameter mixed Model; Salvetti and Banerjee, 1995) for the large eddy simulation.

In present study, the body-force IB method is employed in Nakamura et al. (2008)'s model as the way to assess an external force for the container drifting analysis. In the IB method introduced here, the object is represented as the solid volumetric fraction occupied in each calculation mesh, and the velocity inside the object is controlled by the volumetric fraction. Defining the volume-averaging velocity as $v_i = (1 - F_{ob})v_i^f + F_{ob}v_i^{ob}$ (the solid volumetric fraction of the structure is F_{ob} ($0 \leq F_{ob} \leq 1$); the fluid velocity is v_i^f ; and the velocity of the object is $v_i^{ob} = u_i^{ob} + e_{ijk}\omega_j^{ob}r_k^{ob}$, in which u_i^{ob} is the translation velocity of the object; ω_j^{ob} is the angular velocity of the structure; r_k^{ob} is the relative position vector originated at gravity center of the object; and e_{ijk} is the transposition symbol), governing equations, i.e., a continuity equation (4.1), modified Navier-Stokes equations (4.2) and an advection equation (4.3) of VOF function F ($0 \leq F \leq 1$), employed in present study can be described as follows:

$$\frac{\partial v_j}{\partial x_j} = q^*, \quad (4.1)$$

$$\frac{\partial v_i}{\partial t} + \frac{\partial(v_i v_j)}{\partial x_j} = -\frac{1}{\hat{\rho}} \frac{\partial p}{\partial x_i} - g_i + \frac{f_i^s}{\hat{\rho}} + f_i^{ob} + \frac{\partial}{\partial x_j} (-\tau_{ij} + 2\hat{\nu} D_{ij}) + Q_i - \beta_{ij} v_j, \quad (4.2)$$

$$\frac{\partial F}{\partial t} + \frac{\partial(v_j F)}{\partial x_j} = Fq^*, \quad (4.3)$$

where p is the pressure; x_i is the position vector; t is the time; $g_i = g\delta_{i3}$ is the gravitational acceleration vector, in which g is the gravitational acceleration and δ_{i3} is the Kronecker delta; $\hat{\rho} = (1 - F_{ob})\{\rho_w + (1 - F)\rho_a\} + F_{ob}\rho_{ob}$ is the density, in which ρ_w , ρ_a and ρ_{ob} are the densities of water, air and an object, respectively; $\hat{\nu} = (1 - F_{ob})\{\nu_w + (1 - F)\nu_a\} + F_{ob}\nu_{ob}$ is the fluid kinematic molecular viscosity, in which ν_w , ν_a and ν_{ob} are the kinematic molecular viscosities of water, air and an object, respectively; $q^* = q(y, z, t) / \Delta x_s$ is the wave generation source, in which $q(y, z, t)$ and Δx_s are the source density and x -directional mesh width at a source position ($x = x_s$); f_i^s is the surface tension force based on the CSF (Continuum Surface Force) model; f_i^{ob} is the body force acting on the fluid at the interface and inside the object; τ_{ij} is the turbulent stress based on the DTM (Dynamic Two-parameter mixed Model); $D_{ij} = (\partial v_i / \partial x_j + \partial v_j / \partial x_i) / 2$ is the strain rate tensor; Q_i is the wave source vector; $\beta_{ij} = \beta\delta_{i3}\delta_{j3}$ is the dissipation factor matrix, in which β is the dissipation factor which is equal to zero except for added dissipation zones (Hinatsu, 1992); and the subscripts i and j are governed by the Einstein summation convention. The wave source vector Q_i and the surface tension force f_i^s are formulated as follows:

$$Q_i = v_i q^* - \frac{2}{3} \frac{\partial(\hat{\nu} q^*)}{\partial x_i}, \quad (4.4)$$

$$f_i^s = \sigma \kappa \frac{\partial F}{\partial x_i} \frac{\hat{\rho}}{\bar{\rho}}, \quad (4.5)$$

where σ is the surface tension coefficient; κ is the local surface curvature; and $\bar{\rho} = (\rho_w + \rho_a) / 2$ is the fluid density at the air-water interface. In the present study, the author used the following physical constants: the gravitational acceleration $g = 9.81 \text{ m/s}^2$; the water density $\rho_w = 9.97 \times 10^2 \text{ kg/m}^3$; the air density $\rho_a = 1.18 \text{ kg/m}^3$; the water kinematic molecular viscosity $\nu_w = 8.93 \times 10^{-7} \text{ m}^2/\text{s}$; the air kinematic molecular viscosity $\nu_a = 1.54 \times 10^{-5} \text{ m}^2/\text{s}$; and the surface tension coefficient $\sigma = 7.20 \times 10^{-2} \text{ N/m}$, in which the author adopted the values of $\rho_w, \rho_a, \nu_w, \nu_a$ and σ at 25.0°C and $1.01 \times 10^5 \text{ Pa}$ (National Astronomical Observatory of Japan, 2003).

The reproducing of the turbulent flows in the direct numerical simulation is restricted to low Reynolds numbers because of the need to resolve all spatial scales of turbulence

(Salveti and Banerjee, 1995). In the large eddy simulation (LES), the large-scale field greater than the grid-scale (GS) is directly calculated while the small-scale field called the subgrid-scale (SGS) is modeled with the pioneering Smagorinsky model (Smagorinsky, 1963), dynamic Smagorinsky model (DSM; Germano et al., 1991), dynamic mixed model (DMM; Zang et al. 1993) or dynamic two-parameter mixed model (DTM; Salvetti and Banerjee, 1995). The present study utilized the DTM, in which the SGS stress τ_{ij} is assumed to be proportional to the modified Leonard stress $L_{ij}^m = \overline{v_i v_j} - \overline{v_i} \overline{v_j}$ and the strain rate tensor D_{ij} as follows (Morinishi and Vasilyev, 2001):

$$\tau_{ij}^a = C_L L_{ij}^{ma} - C_S |D| D_{ij}, \quad (4.6)$$

$$C_L = \frac{\mathcal{L}_{ij}^a \mathcal{H}_{ij}^a M_{kl} M_{kl} - \mathcal{L}_{ij}^a M_{ij} \mathcal{H}_{kl}^a M_{kl}}{\mathcal{H}_{ij}^a \mathcal{H}_{ij}^a M_{kl} M_{kl} - \mathcal{H}_{ij}^a M_{ij} \mathcal{H}_{kl}^a M_{kl}}, \quad (4.7)$$

$$C_S = \frac{\mathcal{L}_{ij}^a M_{ij} \mathcal{H}_{kl}^a \mathcal{H}_{kl}^a - \mathcal{L}_{ij}^a \mathcal{H}_{ij}^a \mathcal{H}_{kl}^a M_{kl}}{\mathcal{H}_{ij}^a \mathcal{H}_{ij}^a M_{kl} M_{kl} - \mathcal{H}_{ij}^a M_{ij} \mathcal{H}_{kl}^a M_{kl}}, \quad (4.8)$$

where $|D|$ is the absolute value of the strain tensor D_{ij} ; $\mathcal{L}_{ij} = \widetilde{v_i v_j} - \widetilde{v_i} \widetilde{v_j}$ is the Germano identity; $\mathcal{H}_{ij} = \widetilde{\widetilde{v_i v_j}} - \widetilde{\widetilde{v_i}} \widetilde{\widetilde{v_j}}$; $M_{ij} = \alpha^2 [\widetilde{D} \widetilde{D}_{ij} - |D| \widetilde{D}_{ij}]$; $\alpha = \widetilde{\Delta} / \Delta$, in which Δ and $\widetilde{\Delta}$ are the filter widths of the grid and test scales, respectively; the superscript a represents the anisotropic part of a tensor, e.g., $\tau_{ij}^a = \tau_{ij} - \delta_{ij} \tau_{kk} / 3$; and the subscripts i, j, k and l are governed by the Einstein summation convention. As indicated in Eqs. (4.7) and (4.8), the coefficients C_L and C_S can be dynamically computed with resolved GS velocities v_i . The input parameter in the DTM is only α , and $\alpha = 2.0$ is adopted after Germano et al. (1991).

In present study, the effects of added mass and resistance force are not expected because of absence of the porous media in this numerical analysis, hence descriptions of the coefficient of added mass C_A and the coefficient of resistance force R_i in Nakamura et al. (2008) is omitted here.

4.2.2 Numerical schemes

The SMAC (Simplified Marker And Cell) method (Amsden and Harlow, 1970) is utilized for coupling velocities v_i and pressures p in Eqs. (4.1) and (4.2). Nakamura

et al. (2008) employed the second-order Crank-Nicolson and third-order Adams-Bashforth schemes instead of the standard first-order forward difference scheme for accurate and stable calculations of the time integration of Eq. (4.2), especially the linear resistance force term. In present study, the effect of laminar drag resistance using the Crank-Nicolson scheme can be ignored because of the absence of the porous media. Thus the difference equations lead to:

$$v_i^{p1} = v_i^n + \Delta t^{n+1/2} \left\{ -\frac{1}{\hat{\rho}^n} \frac{\partial p^n}{\partial x_i} - g_i + \left(A_0^n + \frac{\Delta t^{n+1/2}}{2} A_1^n + \frac{(\Delta t^{n+1/2})^2}{6} A_2^n \right) \right\}, \quad (4.9)$$

$$v_i^{p2} = v_i^{p1} + \Delta t^{n+1/2} f_i^{obn}, \quad (4.10)$$

where v_i^{p1} and v_i^{p2} are the predicted seepage velocity vectors in the first and second prediction steps, respectively. The predicted velocity inside objects is corrected to be equal to object velocity, thus the body force acting on the fluid at the interface and inside the object can be written as follow:

$$f_i^{obn} = F_{ob}^n \frac{v_i^{obn} - v_i^{p1}}{\Delta t^{n+1/2}}. \quad (4.11)$$

Using Eq. (4.11), the predicted seepage velocity vectors (Eq. (4.10)) in the second prediction steps are expressed as follow:

$$v_i^{p2} = (1 - F_{ob}^n) v_i^{p1} + F_{ob}^n v_i^{obn}, \quad (4.12)$$

where the superscript n is the time step number; $\Delta t^{n+1/2}$ is the time increment between the n -th and $(n+1)$ -th time steps.

The corrected seepage velocity vectors lead to

$$v_i^{n+1} = v_i^{p2} - \frac{\Delta t^{n+1/2}}{\hat{\rho}^n} \frac{\partial \phi^{n+1/2}}{\partial x_i}, \quad (4.11)$$

where $\phi^{n+1/2} = p^{n+1} - p^n$ is the pressure increment at the $(n+1/2)$ -th time step, which is the following Poisson equation:

$$\frac{\partial}{\partial x_i} \left(\frac{1}{\hat{\rho}^n} \frac{\partial \phi^{n+1/2}}{\partial x_i} \right) = \frac{\partial v_i^p / \partial x_i - q^{*n+1}}{\Delta t^{n+1/2}}. \quad (4.12)$$

And the time-dependent parameters A_0^n, A_1^n and A_2^n are expressed as

$$A_0^n = -\frac{\partial(v_i^n v_j^n)}{\partial x_j} + \frac{f_i^{sn}}{\hat{\rho}^n} + \frac{\partial}{\partial x_j} \left(-\tau_{ij}^n + 2\hat{\nu}^n D_{ij}^n \right) + Q_i^n - \beta_{ij}^n v_j^n, \quad (4.13)$$

$$A_1^n = \left\{ \Delta t^{n-3/2} (\Delta t^{n-3/2} + 2\Delta t^{n-1/2}) A_0^n - (\Delta t^{n-3/2} + \Delta t^{n-1/2})^2 A_0^{n-1} \right. \\ \left. + (\Delta t^{n-1/2})^2 A_0^{n-2} \right\} / \left\{ \Delta t^{n-3/2} \Delta t^{n-1/2} (\Delta t^{n-3/2} + \Delta t^{n-1/2}) \right\}, \quad (4.14)$$

$$A_2^n = 2 \left\{ \Delta t^{n-3/2} A_0^n - (\Delta t^{n-3/2} + \Delta t^{n-1/2}) A_0^{n-1} + \Delta t^{n-1/2} A_0^{n-2} \right\} \\ / \left\{ \Delta t^{n-3/2} \Delta t^{n-1/2} (\Delta t^{n-3/2} + \Delta t^{n-1/2}) \right\}, \quad (4.15)$$

in which TVD (Total Variation Diminishing) scheme of Osher and Chakravarthy (1984) and Chakravarthy and Osher (1985) is used to the convective terms of Eq. (4.13), and the second-order central difference scheme to the other terms of Eqs. (4.9) to (4.15).

For the accurate tracking of air-water interfaces, the advection equation (4.3) was computed with the MARS (Multi-interface Advection and Reconstruction Solver) of Kunugi (2000), one of the PLICs (Piecewise Linear Interface Calculation) such as pioneering PLIC (Youngs, 1982) and TELLURIDE (Rider and Kothe, 1998). In the MARS, the air-water interface in each numerical mesh is described as an inclined plane, which can be easily determined with the neighboring VOF functions F . Detailed explanations of the MARS are available in Kunugi (2000).

In computation of object motion, the aforementioned calculation is firstly performed assuming the object to high viscous fluid ($\nu_{ob} = 1.0 \text{ cm}^2 / \text{s}$), and F is calculated by MARS. Following Xial et al.'s (1997) method, the acting force, then, is computed by using pressure and F_{ob} . The time integration of translational and rotational motions of the object is carried out using the Newmark β method. Furthermore, F_{ob} is calculated based on a linear distance from gravity center. The translational and rotational motions of the object are written as follows:

$$\dot{u}_i^{n+1} = \frac{1}{\rho_{ob}} \sum_{AllCell} F_{ob}^n f_i, \quad (4.16)$$

$$u_i^{n+1} = u_i^n + \Delta t^{n+1/2} \{ \gamma \dot{u}_i^{n+1} + (1 - \gamma) \dot{u}_i^n \}, \quad (4.17)$$

$$x_i^{n+1} = x_i^n + \Delta t^{n+1/2} u_i^n + (\Delta t^{n+1/2})^2 \{ \beta \dot{u}_i^{n+1} + (0.5 - \beta) \dot{u}_i^n \}, \quad (4.18)$$

$$\dot{\omega}_i^{n+1} = \frac{1}{I_i} \sum_{AllCell} F_{ob}^n e_{ijk} r_j^{ob} f_k \Delta x \Delta y \Delta z, \quad (4.19)$$

$$\omega_i^{n+1} = \omega_i^n + \Delta t^{n+1/2} \{ \gamma \dot{\omega}_i^{n+1} + (1 - \gamma) \dot{\omega}_i^n \}, \quad (4.20)$$

$$\theta_i^{n+1} = \theta_i^n + \Delta t^{n+1/2} \omega_i^n + (\Delta t^{n+1/2})^2 \{ \beta \dot{\omega}_i^{n+1} + (0.5 - \beta) \dot{\omega}_i^n \}, \quad (4.21)$$

where $\dot{u}, u, x, \dot{\omega}, \omega$ and θ are the translational acceleration, translational velocity, position of gravity center, angular acceleration, angular velocity and rotational angle, respectively; $f_i = -\partial p^{n+1} / \partial x_i + \rho_{ob} g_i$ is the body force acting on each cell per unit volume; I_i is the inertia moment; and $\beta = 0.3$ and $\gamma = 0.6$ are applied.

4.3 Collision Model

Finite element model is very popular with the users analyzing behavior of structures because of the simplicities for handling and modeling. To date, a large number of commercial codes of finite element model such as MSC.NASTRAN, MSC.DYTRAN, ABAQUS, and ANSYS have been developed, and especially LS-DYNA is representative model for analysis of collision phenomena. DYNA3D originated at the Lawrence Livermore National Laboratory (Hallquist, 1976), and present version, LS-DYNA, was made after repeated improvement (LSTC, 2003). This model is specialized in vehicle collision analysis (e.g., El-Tawil et al., 2005; Elmarakbi et al., 2006), and is capable of FSI (Fluid-Structure Interaction) analysis such as underwater explosion (e.g., Kim et al., 2008), bird striking (e.g., Hanssen et al., 2006) and sloshing inside oil tanker (e.g., Zhang and Suzuki, 2007) as well. The present study utilizes the LS-DYNA in FSI analysis of the drifted container and run-up tsunami, in which ALE (Arbitrary Lagrangian Eulerian; LSTC, 2006) method is used.

4.3.1 Governing equations

LS-DYNA is capable of analyzing fluid-structure interaction by using ALE (Arbitrary

Table 4.1 Characteristics of Eulerian, Lagrangian and ALE methods (Tosaka et al. 2005)

Method	Velocity of mesh (u_i)	Characteristics
Eulerian method	$u_i = 0$ ($w_i = v_i$)	<ul style="list-style-type: none"> ▪ Calculation mesh is fixed in space ▪ Specified study is necessary to reproduce the moving boundary ▪ Calculation mesh is not changed in each time step
Lagrangian method	$u_i = v_i$ ($w_i = 0$)	<ul style="list-style-type: none"> ▪ Calculation mesh is moved in company with fluid particle ▪ Distortion is occurred on the mesh in case of large movement ▪ Alteration of calculation mesh is necessary in each time step
ALE method	$u_i \neq v_i$ ($w_i = \text{arbitrary}$)	<ul style="list-style-type: none"> ▪ Calculation mesh is capable of independently moving from fluid particle velocity ▪ Expression of moving boundary is easy, distortion of mesh can be prevented as well ▪ Altered calculation meshes are reduced because only alteration around moving boundary is enough

Lagrangian Eulerian) method representatively. The standard Lagrangian method has a limitation for reproducing the fluidity body such as water, while the ALE method is capable by using the arbitrary coordinate for that. The standard Lagrangian method assumes that the structure is perfectly loaded the result from the fluid field analysis, in the ALE method, however, the behavior is realistic because of reflected fluid from the structure. In the present study, the author employed the ALE method which is able to efficiently predict the behavior of the run-up tsunami behind the drifted container.

In the ALE method, an arbitrary referential coordinate is introduced in addition to the Lagrangian and Eulerian coordinates. ALE equations (Souli et al., 2000) are derived by substituting the relationship between the material time derivative and the reference configuration time derivative as follow:

$$\begin{aligned}
 \frac{\partial f(X_i, t)}{\partial t} &= \frac{\partial f(x_i, t)}{\partial t} - (v_i - u_i) \frac{\partial f(x_i, t)}{\partial x_i} \\
 &= \frac{\partial f(x_i, t)}{\partial t} - w_i \frac{\partial f(x_i, t)}{\partial x_i}
 \end{aligned}
 \tag{4.22}$$

where X_i is the Lagrangian coordinate; i is the referential coordinate; x_i is the Eulerian coordinate; v_i and u_i are the material (Lagrangian) and reference (ALE) velocities, respectively. In order to simplify the equations, the relative velocity $w_i = v_i - u_i$ is introduced. Eq. (4.22) becomes a Lagrangian expression for $w_i = 0$ ($v_i = u_i$) and an Eulerian expression for $w_i = v_i$ ($u_i = 0$). Characteristics of each calculation method for analysis of moving boundary flows are listed in Table 4.1. Thus the governing equations for the ALE formulation are given by:

(i) The conservation of mass equation

$$\frac{\partial \rho}{\partial t} = -\rho \frac{\partial v}{\partial x_i} - w_i \frac{\partial \rho}{\partial x_i}. \quad (4.23)$$

(ii) The conservation of momentum equation

$$\frac{\partial v}{\partial t} = -(\sigma_{ij,j} + \rho b_i) - \rho w_i \frac{\partial v_i}{\partial x_j}. \quad (4.24)$$

(iii) The conservation of total energy equation

$$\frac{\partial E}{\partial t} = -(\sigma_{ij} v_{i,j} + \rho b_i v_j) - \rho w_j \frac{\partial E}{\partial x_j}, \quad (4.25)$$

where ρ is the density; b_i is the body force; and E is the energy.

At Euler- Lagrangian interface, the Lagrange mesh acts as a moving boundary to the fluid, while fluid pressure is applied to Lagrange mesh. Using penalty coupling allows us to treat the impact problems in presence of fluid because penalty coupling manages the interactions between a Lagrangian formulation modeling the structure and an Eulerian formulation modeling the fluid to flow around a structure but not through a structure. Flow through the structure is prevented in an approximate way by applying penalty forces to the fluid and structure. As soon as an Eulerian node penetrates in a Lagrangian structure, a force of recall is exerted on the contravening node and put back on the surface of the structure.

The constitutive model and equation of state are used to describe fluid-like material model with fluid-like deformation characteristics (air, water, oil, etc.). Constitutive model (CM) relates σ'_{ij} to ε'_{ij} :

$$\sigma_{ij}^v = \sigma'_{ij} = \gamma \dot{\varepsilon}'_{ij}, \quad (4.26)$$

where $\dot{\varepsilon}'_{ij}$ is the deviatoric strain rate; and γ is dynamic viscosity.

Equation of state (EOS) relates pressure (P) to specific rate of change of volume ($\Delta v/v$) of a material at a physical state. In present study, linear polynomial equation (LSTC, 2003) is employed as the EOS, and is given by:

$$P = C_0 + C_1\mu + C_2\mu^2 + C_3\mu^3 + (C_4 + C_5\mu + C_6\mu^2)E, \quad (4.27)$$

where $\mu = -(\Delta v/v) = (\rho/\rho_0) - 1$; ρ/ρ_0 is the ratio of current density to initial density; E is the initial internal energy per unit reference specific volume; $C_1 = 2300 \text{ N/mm}^2$ and $C_0 = C_2 = C_3 = C_4 = C_5 = C_6 = 0$ according to the previous study by Tokura and Ida (2005).

The total stress in the fluid-like material is

$$\sigma_{ij} = \sigma'_{ij} + \frac{1}{3} \sigma_{kk} \delta_{ij} = \gamma \dot{\varepsilon}'_{ij} + P \delta_{ij}. \quad (4.28)$$

4.3.2 Numerical scheme

4.3.2.1 Operating method

Generally, there are two operating methods for applying ALE algorithm. One is that derive a complete interaction equation between object and calculation mesh, and operate. The other is a split operating method used in present study.

The former uses the virtual work equation and follows the ALE approach in the exact sense. It has, however, the defects of increasing operation time because of complicated equations and a large amount of the operation. The latter is the complementary method in the defects of the former. This method is divided into two phases. First a Lagrangian phase is performed, in which the mesh moves with the material, in this phase the changes in velocity and internal energy due to the internal and external forces are calculated. When an excessive displacement occurs on the calculation mesh, the displaced meshes are remapped at the Lagrangian phase back to its original or arbitrary position. In the second phase, the advection phase, transport of mass, internal energy and momentum across cell boundaries are computed.

The overall of an ALE time step is:

1. Perform a Lagrangian time phase.
2. Perform an Advection phase.
 - a. Decide which nodes to move
 - b. Move the boundary nodes
 - c. Move the interior nodes
 - d. Calculate the transport of the element-centered variables
 - e. Calculate the momentum transport and update the velocity

Additionally, calculation process of ALE method used in this study is shown in Fig. 4.1.

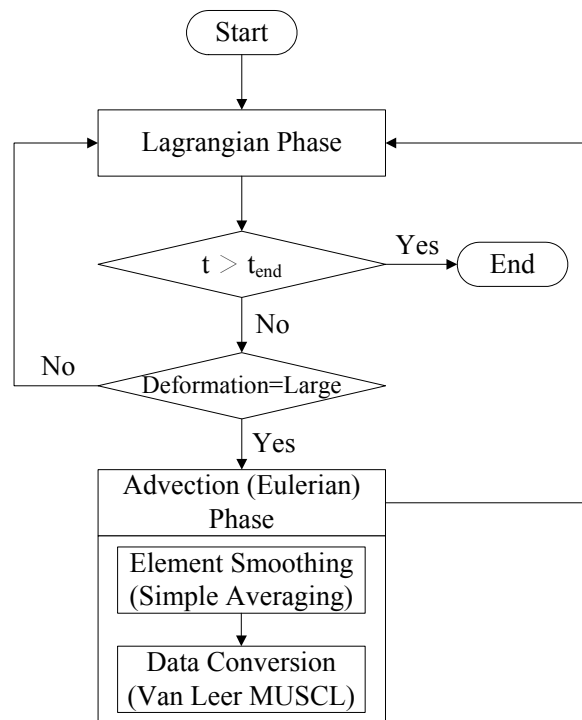


Fig. 4.1 Flow chart of ALE method used in this study

4.3.2.2 Mesh smoothing algorithm

In the advection phase as mentioned above, relative movements of the material and calculation mesh are occurred, and logical and systematic changing method is necessary. Generally the method, that nodes at the boundary are rearranged then internal nodes are placed properly, is used. Since the original smoothing algorithm, the equipotential smoothing of interior nodes, was proposed by Winslow (1990), various algorithms have been proposed and used. LS-DYNA is capable of utilizing following algorithms: equipotential algorithm, simple averaging algorithm, Kikushi's algorithm, surface smoothing algorithm, and combining smoothing algorithms. For simplicity of the

calculation, the simple averaging algorithm in which the coordinates of a node is the simple average of the coordinates of its surrounding nodes is employed in present study and the new location of the node is given by:

$$\vec{x}_{SA}^{n+1} = \frac{1}{m^{tot}} \sum_{m=1}^{m^{tot}} \vec{x}_m^n, \quad (4.29)$$

where m^{tot} is the number of surrounding nodes.

4.3.2.3 Advection algorithm

One of the key points in fluid-structure interaction is the necessity to apply the ALE formulation. This approach is based on the arbitrary displacement of the reference domain which, additionally to the common material domain and spatial domain, is introduced as a third domain. The reference domain correspond the finite element mesh. Hence, the arbitrary movement of the reference frame must be accompanied by reliable mesh moving algorithms, capable to deal with convenient moving boundaries, free surface and large deformations. Thus when applying the ALE formulations, both geometrical as well as advective processes have to be overcome. The donor cell and Van Leer MUSCL (Van Leer, 1977) scheme can be utilized in LS-DYNA. In present study, the Van Lee MUSCL scheme is used to calculate the values of the solution variables (density, interior energy, stress, etc.) in the transport fluxes to achieve second order accurate monotonic results.

The donor cell algorithm assumes that the distribution of ϕ (solution variables) is constant over an element. The Van Leer MUSCL algorithm replaces the piecewise constant distribution with a higher order interpolation function, $\phi_{j+1/2}^n(x)$ that is subject to an element level conservation constraint. The method for obtaining the higher order approximation of the slope is not unique. Perhaps the simplest approach is to fit a parabola through the centroids of the three adjacent elements and evaluate its slope at $x_{j+1/2}^n$. When the value of ϕ at the element centroids is assumed to be equal to the element average this algorithm defines a projection.

$$s_{j+1/2}^n = \frac{(\phi_{j+3/2}^n - \phi_{j+1/2}^n)\Delta x_j^2 + (\phi_{j+1/2}^n - \phi_{j-1/2}^n)\Delta x_{j+1}^2}{\Delta x_j \Delta x_{j+1} (\Delta x_j + \Delta x_{j+1})} \quad (4.30)$$

$$\Delta x_j = x_{j+1/2}^n - x_{j-1/2}^n \quad (4.31)$$

4.3.2.4 Contact condition

In LS-DYNA, thirty-three kinds contact conditions are available. It can be classified roughly into four types, i.e., sliding only, tied interface, slide & void, and single surface. The transaction method of the interface is, furthermore, divided into the kinematic constraint, penalty, and distributed parameter methods. In present study, the Automatic_Surface_To_Surface contact condition, which is used habitually in collision analysis, is employed by using the penalty method as the transaction method of the interface.

The gist of the penalty method is placing a virtual spring in perpendicular between contact node and segment. Stiffness of the spring is calculated at each element on the contact interface, moreover controlling the stiffness parameter is available by user. At first, it checks whether the slave node penetrates the master segment or not. In non-penetration, nothing is calculated, while in penetration, the contact force is loaded on the contact interface. In this moment, the spring is placed on the interface in where this contact force is proportioned to the penetration depth. The contact force f_s loaded on the slave node is:

$$f_s = -lk_i n_i \quad \text{if } l < 0, \quad (4.32)$$

where l is the penetration depth; and n_i is the perpendicular vector on the interface. k_i is the stiffness of the master segment (stiffness of the spring) as follows:

$$k_i = \frac{f_{si} K_i A_i^2}{V_i} \quad (\text{Solid element}), \quad (4.33)$$

$$k_i = \frac{f_{si} K_i A_i}{l_i} \quad (\text{Shell element}), \quad (4.34)$$

where f_{si} is the penalty coefficient (default 0.1); K_i is the bulk modulus; A_i is the area of the segment (face area of the element constituting segment); V_i is the volume; and l_i is the maximum value of thickness and diagonal on the shell element.

Using aforementioned governing equations and schemes, the collision simulation of the drifted container is discussed in next chapters.

4.4 Remarks

For estimating the collision force of drifted container through the numerical experiments, the non-linear finite element program, LS-DYNA, was used in this study. The ALE (Arbitrary Lagrangian Eulerian) method in the LS-DYNA was used for analysis of the container collision under fluid-structure interaction. The biggest weakness of the ALE method is the high calculation load, thus the author employed a coupling system using the drifting model based on IB (Immerged Boundary) method from wave generation to just before the collision and the LS-DYNA during the collision.

As a result, the author obtained the following results:

1. The author referred the IB method of body force type proposed by Yuki et al. (2007), which the object is represented as the solid volumetric fraction in each cell, to the fluid-structure interaction (FSI) analysis. The behavior of a container drifted by the run-up tsunami was examined as incorporating in Nakamura et al.'s (2008) three-dimensional numerical wave flume based on MARS (Multi-interface Advection and Reconstruction Solver).
2. The ALE method (LSTC, 2006) which was able to efficiently predict the behavior of the run-up wave behind the drifted container was employed for the FSI analysis in the LS-DYNA.